Tracing Sagittarius Structure with SDSS and SEGUE imaging and spectroscopy

Brian Yanny[1], Heidi Jo Newberg[2], Jennifer A. Johnson[3], Young Sun Lee[4], Timothy C. Beers[4], Dmitry Bizyaev[5], Howard Brewington[5], Paola Re Fiorentin[6,7], Paul Harding[8], Elena Malanushenko[5], Viktor Malanushenko[5], Dan Oravetz[5], Kaike Pan[5], Audrey Simmons[5], Stephanie Snedden[5]

ABSTRACT

We show that the Sagittarius dwarf tidal stream can be traced with very red K/M-giant stars, selected from SDSS photometry. A subset of these stars are spectroscopically confirmed with SEGUE and SDSS spectra, and the distance scale of 2MASS and SDSS M giants is calibrated to the RR Lyrae distance scale. The absolute magnitude of the K/M-giant stars at the tip of the giant branch is $M_{g_0} = -1.0$. The line-of-sight velocities of the M giant and BHB stars that are spatially coincident with the Sgr dwarf tidal stream are consistent with those of previous authors, reinforcing the need for new models that can explain all of the Sgr tidal debris stream observations. We estimate stellar densities along the tidal tails that can be used to help constrain future models. The K/M-giant, BHB, and F-turnoff stars in the lower surface brightness tidal stream that is adjacent to the main leading Sgr dwarf tidal tail have velocities and metallicities that are similar to those of the stars in the leading tidal tail. The ratio of K/M giants to BHBs and BHBs to F-turnoff stars are also similar for both branches of the leading tidal tail. We show that there is an additional low-metallicity tidal stream near the Sgr trailing tidal tail.

[1]Fermi National Accelerator Laboratory, P.O. Box 500, Batavia, IL 60510

[2]Dept. of Physics, Applied Physics and Astronomy, Rensselaer Polytechnic Institute Troy, NY 12180

[3] Department of Astronomy, Ohio State University, 140 West 18th Avenue, Columbus, OH 43210.

[4]Dept. of Physics & Astronomy, CSCE: Center for the Study of Cosmic Evolution, and JINA: Joint Institute for Nuclear Astrophysics, Michigan State University, E. Lansing, MI 48824

[5]Apache Point Observatory, P.O. Box 59, Sunspot, NM 88349.

[6]Department of Physics, University of Ljubljana, Jadranska 19, 1000 Ljubljana, Slovenia e-mail: paola.refiorentin@fmf.uni-lj.si

[7]Max-Planck-Institut für Astronomie, Königstuhl 17, D-69117 Heidelberg, Germany

[8] Department of Astronomy, Case Western Reserve University, Cleveland, OH 44106.

Subject headings: Galaxy: structure — Galaxy: halo — Galaxy: kinematics and dynamics — Stars: abundances

1. Introduction

Our current model of galaxy formation includes the hierarchical merging of galaxies, first proposed by Searle & Zinn (1978). Evidence for this includes the observation of dwarf galaxies and globular clusters that are even now going through the process of tidal disruption that will eventually assimilate stars from what were once distinct gravitationally bound objects into the Milky Way spheroid. The Sloan Digital Sky Survey (SDSS; Abazajian et al. 2009) and the follow-up SEGUE survey (Yanny et al. 2009) have provided astronomers with a detailed look at tidal disruption of dwarf galaxies and globular clusters in the spheroid of the Milky Way (Yanny et al. 2000; Ivezić et al. 2000; Newberg et al. 2002; Yanny et al. 2003; Grillmair & Johnson 2006; Belokurov et al. 2006a; Grillmair & Dionatos 2006; Belokurov et al. 2006b; Grillmair 2006a,b; Belokurov et al. 2007; Newberg et al. 2007; Grillmair 2008; Willett et al. 2009).

The first significant tidal stream to be discovered, and also the most prominent halo stream, is from the disintegrating Sagittarius dwarf spheroidal galaxy (Ibata, Gilmore, and Irwin 1994; Ibata et al. 2001). The Sagittarius dwarf tidal tails have been traced nearly completely around our Galaxy using 2MASS M-giant stars (Majewski et al. 2003); it is inclined only 13.5° from a polar orbit. Since the shape of the dark-matter potential determines the precession of the tidal-debris orbits, and the lumpiness of the dark matter could scatter stars out of debris streams, the Sgr dwarf tidal debris stream may be an excellent laboratory with which to study the distribution of (presumed) dark matter in and around the Milky Way.

The radial velocities of the M giants in the Sgr tidal stream, however, have presented a puzzle for understanding our Galaxy's gravitational potential. Since Sgr tidal debris is fairly well constrained to a plane, Ibata et al. (2001) and Majewski et al. (2003) have argued that the potential must be close to spherical. On the other hand, Helmi (2004) argues that the debris could be close to the orbital plane in a prolate potential if it was stripped within the last 1.6 Gyr, and that the velocities of the leading tidal tail favor a prolate dark-matter potential. This is further supported by data on RR Lyrae stars from Vivas, Zinn, & Gallart (2005). Other studies have identified stars that are apparently in the trailing tail 80 kpc from the Sun (Newberg et al. 2003), and are near the Sgr orbital plane. This suggests that the potential is nearly spherical or slightly oblate. The leading tidal tail appears to be bifurcated (Belokurov et al. 2006b). Detailed modeling of the Sgr leading tail(s), making the assumption that the smaller of the two streams in the North Galactic Cap is an extension of

the trailing tidal tail, and is thus a full orbit behind the main leading tidal tail, confirm this spherical dark halo finding (Fellhauer et al. 2006). The tilt of the tidal tails with respect to the Sgr orbital plane and other velocities of 2MASS M giants in the Sgr stream, however, suggest that the potential is oblate (Law, Johnston, & Majewski 2005). This puzzle has so far prevented measurement of the even low-order properties of the halo potential.

More data and better models are clearly required. Both photometric imaging, which provides coordinates, estimated distances (from photometric parallax), population information (from colors), and stream stellar densities as a function of position along the stream, as well as spectroscopic information, including radial velocity, kinematics, and metallicity and gravity estimates, are needed for a large set of Sgr stream stars to uniquely constrain an orbit within a potential which may change as a function of radial distance from the Galactic center (Allgood et al. 2006).

Newberg et al. (2007) suggested that there was sufficient confusion in the stellar membership of the stars in the Sgr leading tidal tail that it was possible that the velocities of the leading tidal stars were incorrect. Figure 1 reproduces the stellar density polar plot for photometrically selected SDSS F-turnoff stars ($0.2 < (g - r)_0 < 0.3$, $(u - g)_0 > 0.4$, $21 < g_0 < 22$) from the lower panel of Figure 6 in Newberg et al. (2007), but here we also show the star density in the South Galactic Cap. Using a typical absolute magnitude for the F stars of $M_{g_0} = 4.2$, the Sgr stream is traced for distances of 23 to 36 kpc from the Sun. The Sgr stream disappears on the right side of the top panel where it is further from the Sun, and is faint on the left side of the top panel where it is closer to the Sun. Notice in Figure 1 that there is a clear bifurcation of the Sgr dwarf tidal stream as traced by F-turnoff stars (noted by previous authors) above and below $(l, b) = (255°, 75°)$.

In this paper we isolate stars that are spatially associated with the Sgr leading and trailing tidal tails, and so ensure that the velocities we are measuring are in fact from stars that are part of the tidal debris streams. Using these spatially selected stars, we determine that the velocities from the Law, Johnston, & Majewski (2005) paper are correct, so the puzzle regarding the halo shape still remains.

We show that the velocities, metallicities, and stellar populations in the two pieces of the Sgr dwarf leading tidal tail above and below $(l, b) = (255°, 75°)$ are indistinguishable, which calls into question the assumption that they are different "wraps" of the Sagittarius stream. Newberg et al. (2007) showed that the smaller of the two Sgr leading tidal tails was only slightly farther away than the larger one.

In addition, we show in this paper that K/M giants, color selected in SDSS and SEGUE, can be used to trace distant pieces of the Sgr tidal stream. Majewski et al. (2003) and

collaborators first used this technique with the all-sky 2MASS survey to trace the Sgr tail around the sky to distances of > 50 kpc. We use SDSS and SEGUE spectroscopy of selected K/M giants to confirm their identity as distant giants, rather than nearby M dwarfs or other contaminants. This allows us to make a nearly complete fiducial color magnitude sequence for the Sgr stream in the direction of Virgo/NGP in the SDSS $ugriz$ filter system.

We refine the distance measurement to the Sgr structure by tying the K/M-giant stars to blue horizontal-branch stars (BHBs) and RR Lyraes (Ivezić et al. 2000) previously detected in the same region of the sky. We confirm the result of Newberg et al. (2007) that the leading tidal tail of Sgr stream does not go through the Solar position, but instead passes over the Solar position in the North Galactic cap, and passes through the Galactic plane in the general direction of the Galactic anticenter.

2. Selecting K/M giants in SDSS Filters

We show in this section that we can photometrically select the reddest K/M0-giant stars in the Sgr dwarf spheroidal tidal stream with SDSS ugr filters. M giants are generally metal-rich stars at the tip of the red giant branch, above the point where the horizontal branch intersects the ascending giant branch. They are relatively rare in the Galaxy at high latitude $|b| > 30°$, and are saturated in the SDSS ($r < 14$) if they are closer to the Sun than about 20 kpc. Globular clusters are generally metal poor and therefore have more vertical giant branches in $(g-r)_0, g_0$ color magnitude diagrams. Unfortunately, K giants are difficult to distinguish from K dwarfs based on SDSS $ugriz$ colors alone; a spectrum is required to reliably separate the dwarfs from the giants in the color range $0.5 < (g-r)_0 < 1.1$.

Figure 2 (upper plot) shows a $(u-g)_0$ vs. $(g-r)_0$ color-color diagram of 11,236 SDSS stars with $g_0 < 19$ toward $(l, b) = (330°, 61.5°)$, where the Sgr stream is 44 kpc away (Newberg et al. 2003). This dataset can be reproduced by selecting from the STAR data table of SDSS DR7 [1] all of the objects with $0.9 < (g-r)_0 < 1.6$, $1 < (u-g)_0 < 4$, $200° < \alpha < 210°$, $-1° < \delta < 4°$, and $g_0 < 19$ in the SDSS DR7 database. The SDSS STAR table contains one instance of each point source in the photometric survey. We compare this with a control field (Figure 2, lower plot) that is located at at the same Galactic latitude but at the mirror image position on the opposite side of the Galactic center, $(l, b) = (30°, 61.5°)$, so the number of stars is expected to be similar (except that the Sgr dwarf stream does not pass through that position). The mirror field contains 10,485 stars selected with the same criteria as the Sgr stream field, except with $219° < \alpha < 229°$, $20° < \delta < 25°$. This

---

[1] http://www.sdss.org

diagram clearly shows an excess of red stars below the main sequence in the direction of the Sgr tidal stream. An astute reader will notice that the M-dwarf main-sequence stars are somewhat redder in the control field than they are in the direction of the Sgr stream. That is because all of the stars have been dereddened with the full reddening correction from Schlegel, Finkbeiner, & Davis (1998); since M dwarfs are in front of most of the dust, they have been over-corrected. In the direction of $(l, b) = (330°, 61.5°)$, E(B-V)= 0.028, and in the direction of $(l, b) = (30°, 61.5°)$, E(B-V)= 0.044. Therefore, the M dwarf stars have been over-corrected by a larger amount in the control field, explaining their apparent redder color. The giants, on the other hand, are all at distances well beyond the dust.

In Figure 2 we show two regions of color-color space in which Sgr K/M giants are separated from disk main-sequence stars. The long truncated "diagonal" strip with

$$(u - g)_0 > 3, 1.1 < (g - r)_0 < 1.6, 1.5(g - r)_0 + 1.09 < (u - g)_0 < 1.5(g - r)_0 + 1.59 \quad (1)$$

is most useful for detecting K/M giants at high Galactic latitude. In the SDSS, the photometric errors on u-band become > 0.3 mag at about $u \sim 22$, corresponding to $g \sim 18.5$ for these red stars, which means we can confidently photometrically distinguish the reddest K/M giants from dwarfs out to distances of about 80 kpc from the Sun. At lower Galactic latitudes, there are so many dwarf M stars that even the small fraction that fall at large distances from the locus of dwarf stars make it impossible to distinguish the K/M-giant stars along this whole strip. However, the very reddest stars in the color-color box $1.35 < (g - r)_0 < 1.6$, $3.4 < (u - g)_0 < 4.0$, shown as a rectangle in the lower right of Figure 2, are well separated and can still be used to trace Galactic structure. We explored the possibility of including $r - i$ and $i - z$ information to achieve better separation of the K/M dwarfs and giants, but only tiny improvements to the selection efficiency were obtained.

3. Properties of Sgr K/M giants

Using the color selection technique from the previous section, we are able to select K/M-giant stars in the Sgr dwarf tidal stream, and place them on a Hess diagram similar to that of Figure 5 in Newberg et al. (2002). In that diagram it is not possible to distinguish the M giants due to the more numerous foreground of M-dwarf stars. We selected stars that were on the Sagittarius stream from the same part of the sky that were used in the 2002 version of the figure. One slight difference is that, when the 2002 paper was written, the database was not fully developed, so we used only stars in particular stripes; here we select photometry from objects classified as STAR in SDSS DR7. This slightly changes the epoch of the imaging data used near the stripe boundaries. The Sgr stars are selected with

$200° < \alpha < 225°$, $-1.25° < \delta < 3.75°$, $14 < g_0 < 19.5$, $1.16 < (g - r)_0 < 2.5$, and ugr colors within the diagonal K/M-giant strip cut of Figure 2 (equation 1). Because there are very few spheroid K/M giant stars outside of the Sgr dwarf tidal stream, it was not necessary to perform a background subtraction of stars from regions of the sky that do not contain the Sgr dwarf galaxy.

In Figure 3a, we show the Hess color magnitude diagram for the stars with colors of K/M giants (amplified by 10x) superimposed on the Hess diagram of DR7 stars in the box $200° < \alpha < 225°, -1.25° < \delta < 3.75°$. The gap in K/M stars between $g_0 = 18$ and $g_0 = 19$ supports our contention that the population of photometrically identifed K/M-giant candidates is distinct from that of disk M dwarfs. Figure 3b shows fiducial loci from An et al. (2008) and Clem, Vanden Berg, & Stetson (2008) for the clusters M3 with [Fe/H] $= -1.5$ (cyan), M92 with [Fe/H] $=-2.1$ (blue), and M71 with [Fe/H] ~ -0.8 (red) and shows the spectroscopically confirmed K/M giants in the region of the Sgr Northern leading tail (marked with plus signs and crosses, see section below).

From the relative apparent magnitudes of the K/M-giant stars and the A-type stars in the Sgr dwarf tidal stream, we can calculate the absolute magnitude of these K/M-giant stars. Our previous work (Newberg et al. 2003) shows that the Sagittarius BHB stars in stripes 10 and 11 are at $g_0 = 19.0$, consistent with Figure 3 here. The tip of the red giant branch is at $g_0 = 17.3$ for the stars in this direction, again derived from averaging the stars in Figure 3. If the horizontal-branch stars have an absolute magnitude of $M_{g_0} = 0.7$, then the tip of the M-giant branch in the Sgr dwarf tidal stream is at $M_{g_0} = -1.0$, and $M_{r_0} \sim -2.3$, estimated from the typical M-giant color of $(g - r)_0 = 1.3$. The estimate that BHB stars in our color range have $M_{g_0} = 0.7$ was obtained in Yanny et al. (2000), by converting the absolute magnitude for halo RR Lyrae stars from Layden et al. (1996) into the g filter, and noting that the BHB stars are about the same absolute magnitude as the RR Lyrae stars. Since this determination rests on several approximate steps our distance scale is not absolute, however, it enables measurement of the relative magnitudes of the different types of stars that have been used as distance indicators in the Sgr stream.

Note here that Chou et al. (2007) measured a metallicity gradient along the tails of the Sgr dwarf tidal tails that could affect the average absolute magnitude of K/M giants as a function of position on the stream. This gradient is in addition to the scatter in absolute magnitude for these stars that arises due to surface gravity and metallicity differences between stars in the same stream position. We attempted to confirm the metallicity gradient by measuring the difference in apparent magnitude between the BHB stars and the K/M-giant stars as a function of position along the stream, but were unable to form any firm conclusions because the stream is not well- separated from foreground stars by photometry for most of

the length of the stream (see Figures 6 and 8), and the vast majority of the spectra are within a 30° piece of the stream at $270° < \Lambda_\odot < 300°$ (see section 8). The difference in apparent magnitude between the BHB and K/M-giant stars was calculated for Sgr stream stars with $240° < \Lambda_\odot < 270°$ and with $270° < \Lambda_\odot < 300°$. This apparent magnitude difference was about 1.7 magnitudes for $240° < \Lambda_\odot < 270°$ and 1.6 magnitudes for $270° < \Lambda_\odot < 300°$, but consistent with no metallicity change over this section of the tidal stream. It should be noted that we are using primarily photometrically selected M-giant candidates in this study, so the results are likely to be affected by the presence of many K giants in the tidal debris. This study needs to be repeated with many more spectra of both BHB and M giants.

Next we attempt to fill in the Sgr giant branch in the $0.7 < (g - r)_0 < 1.1$ region by selecting spectra of stars with radial velocities that are the same as other stars in the Sgr stream. We selected Sgr giant branch candidates from all of the spectra in SDSS DR7 with $200° < \alpha < 225°$, $-1.25° < \delta < 3.75$, $\log g < 4.0$, $0.4 < (g - r)_0 < 1.6$, $g_0 < 19.5$, and $26 < v_r < 56$ km s^{-1}. This selection netted 51 candidate K/M-giant spectra, which we then examined individually by eye. Thirty-three of the stars we classified as K/M giants; the other stars were G stars and M dwarfs. Note that this exercise was done to determine the colors and magnitudes of K and M giants the the Sgr dwarf tidal stream, and not to assess the general success of the color selection in identifying giant-branch stars. Of the 51 candidate K/M-giant stars, 25 are in the ugr diagonal K/M-giant color selection box. Of those twenty-five, one is an M dwarf, 9 are K giants, and 15 are M giants, but recall that these stars were also pre-selected on surface gravity and velocity. A better way to assess the contamination of the Sgr K/M-giant sample is to compare the density of stars in the stream to the density of stars in the field in Figures 2 and 6. In Figure 2, there are 94 K/M-giant star candidates in the Sgr dwarf tidal stream and 30 in the off-stream field, suggesting that 68% of the selected stars in this region are actually members of the Sgr stream. Of these, about 60% are expected to be M giants rather than K giants. In Figure 6, one can see that the background contamination increases close to the Galactic plane, so the fraction of stars that are in the stream will be lower.

In Figure 4 we show two selected Sgr K/M-giant tidal stream spectra, plus, for comparison, one spectrum that we classified as an M dwarf. The stars were classified as M dwarfs if they had a strong and narrow Na absorption line, the Mg triplet at 5200Å was prominent, and there was strong Ca at 4226Å; otherwise we classified it as a giant. We saw two distinctly different types of giant spectra, as can be seen by comparing the top two spectra in Figure 4. Stars with strong TiO bands, which we identify as M giants, as seen in the second spectrum in Figure 4, are shown as plus signs in Figure 3b. Stars with spectra more like the top spectrum in Figure 4 tended to be bluer, and are K giants, as represented by the crosses in Figure 3b.

The giant stars in the Sgr stream were plotted on the Hess diagram in Figure 3b, allowing us to better trace the Sgr giant branch. The giant branch, which previously couldn't be seen redder than $(g - r)_0 > 0.6$, is now completed from $(g - r)_0 = 0.75$ to 1.6. We verified that the color-magnitude diagram for the stars that we spectroscopically identified as G stars and M dwarfs does not show a coherent giant branch, validating our ability to correctly classify the SDSS spectra.

Comparison of the fiducial SDSS photometric sequences of known globular clusters (An et al. 2008) indicates that the BHB stars in the Sgr tidal stream have metallicities of $-2.3 < [\text{Fe/H}] < -1.6$. RR Lyraes in the Northern leading tail have metallicities of $[\text{Fe/H}] = -1.76 \pm 0.22$ as shown by Vivas, Zinn, & Gallart (2005). The Stellar Structure Parameters Pipeline (SSPP) (Lee et al. 2008a,b; Allende Prieto et al. 2008) generates metallicities for all stars in SDSS + SEGUE (over the color range $0.3 \le (g - r)_0 \le 1.3$, and with spectra of sufficient signal-to-noise); the 33 Sgr K/M-giant stars have $[\text{Fe/H}] \sim -0.8 \pm 0.3$. We note that the absolute metallicity determinations of the SSPP are not well-calibrated for M giants. However, Chou et al. (2007) have obtained high-resolution metallicities of some Sgr stream M giants in this part of the sky, and find metallicities consistent with these values.

4. Comparison of Sgr K/M giants in SDSS and 2MASS

We obtained infrared photometry from the 2MASS catalog (Skrutskie et al. 2006) for each of the Sgr K/M-giant stars selected in the previous section, using the matching program from the US National Virtual Observatory. Figure 5 shows stars $(J-K_S)_0$, $(J-H)_0$ colors of the K/M giant candidates selected from ugr photometry, both for the strip cut and the very red box that can be used at low Galactic latitude. The 2MASS colors have been dereddened using the procedures described in Majewski et al. (2003). In the same figure we show JHK_S photometry for spectroscopically confirmed Sgr K and M giants, and the JHK_S selection box used by Majewski et al. (2003) to select K and M giants from Sgr over the entire sky.

Examining Figure 5 in detail, we note that the 2MASS $(J - H)_0$ color is good at separating dwarfs with $0.4 < (J - H)_0 < 0.7$ from giants with $0.7 \le (J - H)_0 < 0.95$, while $(J - K)_0$ can be additionally used to somewhat separate K giants with $0.8 < (J - K)_0 < 1.0$ from M giants with $1.0 < (J - K)_0 < 1.2$.

We select similar K- and M-giant candidates to the Majewski et al. (2003) selection, but the population of K and M giants selected optically in ugr by the diagonal strip cut of Eq. 1 includes some bluer stars in $J - H, J - K$, while the very red SDSS ugr selection box of Figure 2 excludes most of the stars on the blue side (in $J - K$) of the Majewski et al.

(2003) selection box.

5. Tracing Sgr in K/M Giants

Now we select K/M-giant candidates via the strip color cut (Eq 1) over the whole of the SDSS+SEGUE imaging area. We used only regions of the sky with low reddening ($E(B-V) < 0.25$). In order to eliminate some of the nearby disk M dwarfs from the sample, we eliminated stars from the sample if they had proper motions of more than 6 mas yr^{-1} (note that $|\mu_b| > 6$ and $|\mu_l| > 6$ mas yr^{-1} is required if a proper motion is measured at all in the SDSS DR7 proper motions table, where the typical proper motion error for a star is typically 3 mas yr^{-1}). Using an estimated distance to each giant candidate assuming the absolute magnitude is $M_{g_0} = -1$, as determined in §3, and also using the definition of the Sgr dwarf coordinate system as defined by Majewski et al. (2003), we convert (l, b) and distance to $(X_{Sgr}, Y_{Sgr}, Z_{Sgr})$ for all K/M-candidate giant stars. In this coordinate system, the axes X_{Sgr} and Y_{Sgr} are in the Sgr dwarf spheroidal orbital plane, and are not far from the Galactocentric X and $-Z$ coordinates, respectively. The Z_{Sgr} coordinate direction is perpendicular to the Sgr dwarf orbital plane, and is approximately in the Galactocentric $+Y$ direction.

Figure 6a shows 5,402 stars within 5 kpc of the Sgr dwarf orbital plane, $|Z_{Sgr}| < 5$ kpc. The leading Sgr tail arcs over the Sun's position and intersects the plane of the Milky Way at approximately $X_{Sgr} = -25$ kpc (the Sun is at -8 kpc, so that is about 17 kpc from the Sun). Additionally, candidate Sgr K/M giants south of the plane are clearly present. The positions of these stars are consistent with the positions of BHB stars in Figure 1 of Newberg et al. (2007).

Our next step is to spatially isolate those stars that are in the Sgr stream in three dimensions. Part of the motivation for this is to separate the Sgr members from the closer Virgo stars, a very confusing region of the halo with likely several structures present (Vivas et al. 2001; Jurić et al. 2008; Newberg et al. 2007; Keller, Da Costa, & Prior 2009).

We draw two parabolic arcs to define the limits of the leading tidal tail: $Y_{Sgr} < 0$, $0.025(X_{Sgr} - 11)^2 - 53 < Y_{Sgr}$, and $Y_{Sgr} < 0.028(X_{Sgr} - 8)^2 - 32$, where all distances are in kpc. In the south Galactic cap we selected stars in the trailing tidal between the parabolas defined by: $Y_{Sgr} > 0$, $-0.16(X_{Sgr} + 10)^2 + 16 > Y_{Sgr}$, and $Y_{Sgr} < -0.010(X_{Sgr} + 18)^2 + 35$. Figure 6b shows in red the 472 candidate K/M-giant stars that were selected in the region of the leading tidal tail, and the 133 candidate K/M-giant stars that were selected in the region of the trailing tidal tail.

Figure 7 shows the (l, b) positions of the final set of candidate K/M-giant stars that are spatially coincident with the Sgr dwarf tidal stream defined by the annular cuts above. The upper panel shows positive b and the lower panel shows negative b (below the Galactic plane). The light gray shading represents the sky covered by the SDSS and SEGUE imaging surveys. The darker black regions represent areas where the Sgr tidal stream stars are present. Since the stars were selected to be at the same distance as the Sgr stream, and within 5 kpc of the Sgr orbital plane, the footprint of the stream on the sky is narrower on the right side of the figure where the stream is 50 kpc away, and wider on the left side where the stream is only 20 kpc away from the Sun. We do not see a bifurcation of the Sgr stream in this figure, though this can be easily accounted for by the low numbers of of K/M-giant candidates.

6. Sgr Traced in A Stars

We now do the same analysis as performed for the K/M stars, except we choose photometrically selected BHB stars, which are also very prominent in the Sgr tidal streams. The A-type stars were selected from the SDSS DR7 STAR database, with $15 < g_0 < 21$, $-0.3 < (g - r)_0 < 0.0$, and $0.8 < (u - g)_0 < 1.5$. An additional color cut in ugr was applied that separates these blue stars into those that are more likely to be high surface-gravity stars and those that are likely to be low surface-gravity BHB stars (Yanny et al. 2000; Newberg et al. 2007). Just as in the K/M-giant candidate selection, we eliminated stars with proper motions larger than 6 mas yr^{-1} and in areas of the sky with $E(B - V) < 0.25$. The positions of the 32,881 BHB stars within 5 kpc of the Sgr dwarf tidal stream are shown in Figure 8a.

Because the K/M-giant candidate selection is cleaner (the photometrically selected BHBs have significant contamination from blue-straggler stars and BHBs in the spheroid), the spatial selection for leading and trailing tail BHB stars was chosen to be identical, assuming the candidate K/M giants are at $M_{g_0} = -1.0$ and the BHBs are at $M_{g_0} = 0.7$. Figure 8b shows in red the positions of all the selected BHBs that are in the same areas of sky as the candidate K/M giants in Figure 6b, but with g_0 limits that are shifted by 1.7 magnitudes.

We note several interesting features in Figure 8 in the region beyond 40 kpc from the Sun. There is a significant group of BHBs at about 80 kpc from the Sun, near $(X_{Sgr}, Y_{Sgr}) = (-80, -40)$ kpc, which are believed to be associated with the Sgr stream, and have been discussed in detail by Newberg et al. (2003). Additionally, in their study of the Sagittarius stream, Belokurov et al. (2006b) note distant ($d \sim 50$ kpc) structures manifesting themselves as double sub-giant branches in color-magnitude diagrams along the stream. The fainter turnoffs which they note at $180° < \alpha < 190°$ correspond roughly to the overdensity of BHB

points at $(X_{Sgr}, Y_{Sgr}) = (-10, -50)$ kpc, behind the main upper branch of the Sgr stream at $(X_{Sgr}, Y_{Sgr}) = (-10, -30)$ kpc.

Figure 9 shows the (l, b) polar plots of BHB stars selected in Figure 8b that are within 5 kpc of the Sgr dwarf orbital plane. The density pattern is very similar to the density pattern for candidate K/M giants shown in Figure 7. The bifurcation is not apparent, probably because the star counts are not high enough to see the two streams clearly. The dark spot on the left side of the top panel in Figure 9 near $(l, b) = (185°, 25°)$ is a lower latitude region where the Monoceros stream is also present at these distances ($d \sim 20$ kpc) from the Galactic plane. Thus we are not certain of the association of this BHB overdensity with the Sgr stream.

7. Sgr Traced in F Stars

The F-turnoff stars are also selected for comparative analysis. They are more numerous, but we begin to lose sensitivity to these intrinsically fainter stars in the SDSS at distances beyond 40 kpc from the Sun, so we do not sample the most distant parts of the stream in the North Galactic Cap. We photometrically selected F-turnoff stars from the SDSS DR7 STAR database with $0.1 < (g - r)_0 < 0.3$, $19 < g_0 < 24$, $-6 < \mu_l < 6$, $-6 < \mu_b < 6$ mas yr^{-1}, $E(B - V) < 0.25$, and $-5 < Z_{Sgr} < 5$ kpc, where the conversion from (l, b, g_0) to $(X_{Sgr}, Y_{Sgr}, Z_{Sgr})$ assumes $M_{g_0} = 4.2$. We also eliminated stars near the globular clusters M 53 and NGC 5053 by eliminating stars in the region $331° < l < 337°$ and $79° < b < 81°$. This results in a sample of 710,832 stars. Figure 10 shows the density of F-turnoff stars in the Sagittarius orbital plane. The Sgr stream artificially appears much broader in F-turnoff stars, since these stars have a wider range of absolute magnitudes; when we calculate each star's position we assume a single, average, absolute magnitude so there are large distance errors in the positions of these stars in Figure 10. In the upper right corner of this diagram we lose most of the stars in the Sgr dwarf tidal stream because they are too distant to be seen in SDSS data. The background counts of F-turnoff stars are very high near the Sun, and those with $g_0 < 19$ are removed from the figure.

Nevertheless, we select F-turnoff stars $|Z_{Sgr}| < 5$ kpc as we selected BHB and candidate K/M-giant stars in the previous two sections. Because there are much larger distance errors, we select a somewhat smaller fraction of the Sgr F-turnoff stars this way. The 223,977 stars that are positionally coincident with the Sgr stream are shown in Figure 11. Even though we lose the Sgr stream at large distances, on the right side of the upper panel, we do not lose them as quickly as for the magnitude-limited sample in the upper panel of Figure 1. The larger number of F-turnoff stars allows us to see the bifurcated leading tidal tail above

and below $(l, b) = (255°, 75°)$. Some SDSS striping, an artifact of the SDSS's photometric calibration near its magnitude limit $g \sim 23.5$, is seen in the density distribution of the upper panel of Figure 11.

8. Velocities along the Sgr Stream

We now select stars that are positionally coincident with the Sgr leading and trailing tidal tails, and plot their line-of-sight, Galactic standard of rest velocity, $v_{gsr} = \text{rv} + 10.1 \, cos \, b \, cos \, l + 224.0 \, cos \, b \, sin \, l + 6.7 \, sin \, b$ km s^{-1}, where rv is the heliocentric radial velocity, as a function of position along the stream, $\Lambda_\odot$. We selected from SDSS DR7 all of the SDSS/SEGUE velocities for K/M-giant stars in Figure 7 for which spectra exist. Neither SDSS nor SEGUE targeted giant stars this red; most of the 55 selected K/M-giant spectra are from a small set of special plates in a very restricted part of the sky. Since we have spectrally determined surface-gravity information for horizontal-branch (HB) stars that will allow us to distinguish them from the much more numerous F dwarfs, we can select HB-star spectra with a much broader color range that we used to photometrically select the BHB stars in Figure 9. The spectroscopically selected BHB-star sample includes all SDSS DR7 spectra of point sources with $-0.3 < (g-r)_0 < 0.35$, $0.8 < (u-g)_0 < 1.5$, $1.0 < \log \text{g} < 3.75$, and $-5 < Z_{Sgr} < 5$. The annular cuts of §5 are performed. Using these criteria, 999 HB stars were selected.

We show in the upper panel of Figure 12 a plot similar to that of Law, Johnston, & Majewski (2005) Figure 12, showing the Galactocentric, line-of-sight velocity of all K/M giants with radial velocity information, as well as the 999 HB stars with velocities, as a function of angle along the Sgr tidal stream. The heliocentric angle along the stream, $\Lambda_\odot$, is the same as used above.

When we initially made Figure 12, we noticed that the velocities of the HB stars near $\Lambda_\odot = 100°$ did not match the velocities measured in the Law, Johnston, & Majewski (2005) paper. We looked at the metallicities of the BHB stars and determined that in the South Galactic Cap, near $\Lambda_\odot = 100°$, there was a cluster of BHBs with lower metallicities than the other Sgr BHB stars, and higher v_{gsr} than the other Sgr K/M giants and BHBs. Therefore, we split the BHBs into higher metallicity ([Fe/H]$_{\text{WBG}} > -1.9$) and lower metallicity [Fe/H]$_{\text{WBG}} < -1.9$ subsets. The WBG subscript refers to the technique of estimating metallicity for a blue star based on its estimated T_{eff} and Ca K line strength of Wilhelm, Beers, & Gray (1999). The SDSS SSPP measures metallicities by several techniques, and includes an 'FeHa' ([Fe/H] adopted) average metallicity that is generally accepted as the best overall measure of metallicity. However, we have found that the WBG

metallicity, which was developed specifically for BHB stars, is a better measure for these blue stellar types, so we use that measure for HB stars throughout this paper.

The K/M giants and the higher-metallicity BHB stars trace the Sgr dwarf tidal stream, and are a good match to the velocities determined by Law, Johnston, & Majewski (2005). The low-metallicity BHB stars, while they are at a similar apparent distance as the Sgr dwarf tidal stream, have distinct velocities in the trailing tidal tail (upper panel of Figure 12). In the North Galactic Cap, there are many high- and low-metallicity BHB stars with a broad range of velocities, as one would expect in the spheroid, the K/M giants and some of the higher-metallicity BHB stars follow the Sgr stream, and there is a cluster of stars with zero or slightly negative v_{gsr} at $\Lambda_\odot = 190°$ (which are presumably associated with the Monoceros stream complex, or a distorted disk, that is found at low Galactic latitude near the anticenter).

Spectra of stars in the field associated with the globular clusters NGC 5053 and M 53, which overlaps the Sgr north high-latitude branch, are explicitly removed from this study.

In the Sgr stream we find both low- and high-metallicity BHB stars. Note the very low-metallicity BHBs in the Virgo Overdensity at $\Lambda_\odot = 230°$, $v_{gsr} = 130$ km s^{-1} in the upper panel of Figure 12. Additionally, a close examination of spectra associated with density enhancements in the lower panel of Figure 9, where the Sgr stream crosses near the South Galactic Pole, also shows a second stream, apparently independent of Sagittarius, and not in the Sgr plane, of very low-metallicity stars ([Fe/H] ~ -2). These low-metallicity stars will be explored in a forthcoming paper (Newberg, Yanny & Willett 2009).

Figure 13 highlights the metallicity difference used to help identify this apparent additional population, distinct from Sgr in the south. Figure 13(a) contains two outlined boxes. The rectangular box has 22 high-metallicity BHBs (black dots) and 41 low-metallicity BHBs (blue crosses), a ratio of 1:2 high:low. The diagonal Sgr box, however, has 60 high-metallicity BHBs and 37 low-metallicity stars, for a reverse ratio approaching 2:1. The distances to the objects are shown in Figure 13(b), where the objects in the rectangular (non-Sgr) box are presented as (green) triangles (low metallicity) and squares (high metallicity). Here too, the distribution of the low-metallicity BHBs in the rectangular at 30 kpc appears distinct from that of the higher-metallicity stars in Sgr, which slopes from d=20 kpc to d=30 kpc as $\Lambda_\odot$ increases from 75° to 120°.

The Sgr BHB stars and the K/M-giant stars with SDSS and SEGUE spectra trace the Sgr dwarf tidal stream with essentially the same velocities as those measured by Law, Johnston, & Majewski (2005), using stars that follow the density enhancement of the the Sgr stream. The conjecture put forth by Newberg et al. (2007) that the Sgr stream velocities in Law, Johnston, & Majewski

(2005) might have been measured for stars at the wrong distance appears to be incorrect. Therefore, it remains a challenge to fit a model for Sgr dwarf tidal disruption to the measured velocities in the leading tidal tail.

9. Analysis of the "Bifurcated" leading tidal tail

In this section we compare spectra of the stars in the two tidal debris streams identified by Belokurov et al. (2006b), and apparent in the top panel of Figure 1. In the North Galactic Cap, the two pieces of the stream can be separated in Z_{Sgr}. Figure 14 (upper panel) shows the positions of all of the SDSS and SEGUE spectroscopically selected HB stars, as selected in the previous section, (and shown in Figure 12) that have $-5 < Z_{Sgr} < 5$ kpc. The smaller debris stream at higher Galactic latitude, $Z_{Sgr} > 0.04X_{Sgr}+1.0$, is shown as cyan dots in the figure. The larger debris stream, $Z_{Sgr} < 0.04X_{Sgr}+1.0$, is shown as magenta dots. Although the larger stream at lower Galactic latitude has more stars, and presumably more HB stars, it is more sparsely sampled.

Figure 15 shows all of the stars in Figure 12 that are in the higher Galactic latitude piece of the leading tidal tail, and Figure 16 shows all of the stars in Figure 12 that are in the lower Galactic latitude piece of the leading tidal tail.

The K/M giants in both the Northern and Southern branches have velocities that are consistent with the full set of spectra. The difference in the $\Lambda_\odot$ positions of the concentration of K/M giants in each branch is a selection effect in the data and not due to any intrinsic difference between the streams. In the lower panels of Figure 15 and 16, we see that the K/M giants in the higher Galactic latitude stream are on the closer side of the selection box, while the K/M giants in the lower Galactic latitude stream are on the further side of the selection box. In contrast, Newberg et al. (2007) found that the northern branch was farther away at $\Lambda_\odot \sim 220°$. This suggests that the two pieces of the stream cross each other in distance.

There is also no difference in the velocities of the Sgr BHB stars as a function of $\Lambda_\odot$. Since the more northern branch of the leading tidal tail is extremely low surface brightness in the region $180° < \Lambda_\odot < 240°$, the Sgr stream is not apparent in Figure 15 in this region.

In the lower panel of Figure 14 we show all of the spectra from the upper panel that also have the velocities of the Sgr dwarf leading tidal tail. These were selected as stars that have $0.10(\Lambda_\odot - 200°)^2 - 150 < v_{gsr} < 0.17(\Lambda_\odot - 200°)^2 - 90$ km s^{-1}, and $180° < \Lambda_\odot < 300°$. This cut eliminates most of the spectra at low Galactic latitudes near the Galactic anticenter, most of the spectra on the Orphan Stream, and most of the spectra that are not aligned

with photometric overdensities of F-turnoff stars in Figure 14.

10. Metallicities of the Sgr BHB stars

It was shown in Harrigan et al. (2009) that, by comparing BHBs in globular clusters with published globular cluster metallicities, that the SSPP WBG metallicities for BHB stars were reasonable, but possibly a tenth of a dex too high. Here, we would like to compare the BHB stars in the two branches of the leading Sgr tidal tail, doing an internal comparison to see if the metallicities are different. This check is independent of any overall offset in the metallicities determined by SSPP, which could be a few tenths of a dex.

In Figure 17, the upper panel shows the distribution of metallicites of the HB stars in Figure 14 (lower panel). These stars were divided into those that have the velocities of the Sgr leading tidal tail, as used to select the spectra in the lower panel of Figure 14, and those which were in the upper panel but did not have velocities of the Sgr leading tidal tail. The Sgr BHB spectra were further divided by branch of the leading tidal tail (cyan and magenta points in Figure 14 for the upper and lower branches respectively). Note that both the upper and lower branches of the Sgr leading tidal tail stars have similar metallicity distributions. The HB stars that do not have the correct velocities are spread in a much broader range of metallicities, as one would expect from a background spheroid population (black line in upper panel of Figure 17). The Sgr dwarf BHBs in both branches of the leading tidal stream have metallicities $-2.3 < \mathrm{[Fe/H]_{WBG}} < -1.6$. Since the BHBs are expected to trace only the older, more metal poor component of the Sgr dwarf galaxy, these stars do not represent the entire range of metallicities in the stream. Some of these stars may in fact overlap the RR Lyrae sample studied by Vivas, Zinn, & Gallart (2005) in the Northern Sgr leading tidal stream. Our determination of HB metallicity (as well as velocity) is consistent with their determination of $\mathrm{[Fe/H]} = -1.76 \pm 0.22$.

The lower panel of Figure 17 justifies our definition of 'higher' and 'lower' metallicities in Figure 12. The metallicity distribution of the BHB stars with velocities of the trailing Sgr tidal stream ($70° < \Lambda_\odot < 108°$, $-2.0\Lambda_\odot + 60 < v_{gsr} < -2.0\Lambda_\odot + 120$ km s^{-1}) are similar to the metallicities of both branches of the Sgr leading tidal tail. On the other hand, stars selected with velocity ($-71 < v_{gsr} < 0$ km s^{-1}) and $\Lambda_\odot$ ($85° < \Lambda_\odot < 140°$) are consistent with the new debris stream discovered in the South Galactic Cap have a lower metallicity (see Figure 13).

Bellazzini et al. (2006) showed that the ratio of BHB to red-clump stars is higher in the stream vs. the bound core of Sgr, indicating that the stream stars are from a more

metal-poor population of stars that was less tightly bound and thus was stripped first. We studied the metallicity of the BHB stars as a function of $\Lambda_\odot$, and find that there is no significant trend in BHB metallicity vs. $\Lambda_\odot$, at least along these portions of the tidal stream ($100° < \Lambda_\odot < 115°$, $200° < \Lambda_\odot < 300°$). Note that since all BHB stars have low metallicity, it is unclear that one would expect a trend in the metallicities of BHB stars even if there is a metallicity gradient along the stream (Chou et al. 2007).

11. Densities along the Sgr Stream

Figures 7, 9, and 11 graphically show the density of K/M-giant, BHB, and F- turnoff stars, respectively, along the Sgr dwarf tidal tails. Note that the number counts in BHB and K/M-giant stars are much higher on the right sides of these figures in the North Galactic Cap, both because the stream density is higher at apogalacticon and because the stream is farther away, so each pixel, which represents a fixed angular area in the sky, intersects a larger linear distance along the stream. In this section, we construct histograms of the number counts of these three types of stars along the Sagittarius stream.

We plot in Figure 18 the number density of photometrically selected Sgr candidate K/M-giant, BHB and F-turnoff stars, selected as a function of angle along the Sgr dwarf tidal stream, $\Lambda_\odot$, as defined in Majewski et al. (2003). Figure 18(a) shows the star counts from Figures 7, 9 and 11 as a function of $\Lambda_\odot$.

In Figure 18(b), we correct the star counts for the fraction of the width of the stream we observe, subtract the background counts, and divide by the distance to the stream. To estimate the fraction of the stream width that we observe in each ten-degree slice of $\Lambda_\odot$, we first estimate the density of objects on the sky within the SDSS footprint by using quasar number counts as a constant density reference tracer (Yanny et al. 2000). We select QSOs over the whole sky from the SDSS DR7 STAR data base which had $-0.05 < (u-g)_0 < 0.4$, $-0.1 < (g-r)_0 < 0.3$, and $18 < g_0 < 21$. At each $\Lambda_\odot$ bin, we estimated the angular cross section, θ, of the stream from its distance ($\theta = 5$ kpc/d). In addition to the longitude-like angle $\Lambda_\odot$ along the Sgr stream, Majewski et al. (2003) also defined a latitude-like angle $B_\odot$ that we will use to measure the angle across the stream. We counted all QSOs in the $\Lambda_\odot$ range that were also within the $-\theta < B_\odot < \theta$ limits. The fraction of the stream sampled by our data is given by the number of QSOs in the ($\Lambda_\odot$, $B_\odot$) bin, divided by the number of QSOs we would have expected. The expected number of QSOs is the typical number of QSOs per square degree, multiplied by ten degrees of $\Lambda_\odot$, and then multiplied by 2θ. The normalization factor, multiplied by 20, is indicated by the small circles in Figure 18. For example, if the normalization circle is at "20", there is no correction factor applied. If

the circle is at "60," then the number counts are multiplied by three. If the stream is not uniform density in cross section within 5 kpc of the Sgr orbital plane, then this correction is not perfect. In general, $\Lambda_\odot$ bins with data in the center of the stream but not the edges are over-corrected, and bins with data at the edges of the stream but not in the center are under-corrected.

To estimate the background counts, we divided both the BHB star sample and the K/M giant sample into distance bins that were 5 kpc deep (0-5 kpc from the Sun, 5-10 kpc from the Sun, etc.), and then for each type of star and each distance range we constructed binned star counts. We estimated the background from the portions of the histograms that were away from the Sgr stream, and not at very low Galactic latitude. These estimates were done only in the North Galactic Cap where we had full sky coverage, but were applied to both the northern and southern data sets. To find the background in the entire distance range of the Sgr stream selection, we numerically integrated the star counts over each of the 5 kpc deep bins that overlapped the area between the two parabolas that were used to select the stream stars, for each $\Lambda_\odot$ bin. The total background counts was then subtracted from the corrected star counts. If the background subtraction resulted in negative stream density, then that bin is suppressed in Figure 18.

In a fixed angular distance along the stream, we intersect a larger linear distance along the stream. Therefore, after correcting for completeness and background we divided the counts in each bin by the distance to the stream for each $\Lambda_\odot$ bin. Therefore, the counts in each bin are an estimate of the number of stars along the stream, per kpc projected perpendicular to our line of sight.

Figure 18(b) shows that the K/M-giant and BHB star counts fall quite rapidly from $\Lambda_\odot = 300°$ to $\Lambda_\odot = 250°$, as we move away from one of the stream's apogalactic orbital 'turning points' where stars are expected to pile up in density. The F-turnoff star number counts are low near $\Lambda_\odot = 300°$ because F-turnoff stars at the distance to the Sgr stream there are too faint to be observed in the SDSS. We expect that the actual counts of F stars have similar density patterns to the K/M-giant and BHB stars. There are about 50% more BHB stars than K/M giants in the leading tidal tail, and about 300 times as many F-turnoff stars as BHBs. In the south, the numbers are less certain because the correction factors are larger. The number counts for all three types of stars are approximately constant in the range $60° < \Lambda_\odot < 115°$. It is plausible that the ratios of K/M giants to BHBs to F-turnoff stars is the same in the trailing tail as in the leading tail. In both the leading and trailing tidal tails, the BHB star counts show more bin-to-bin fluctuations than the K/M-giant star counts.

The last two panels of Figure 18 are similar to the second panel, except they give star

counts for the upper, c), and lower, d), branches of the leading tidal tail only, with the split at $Z_{Sgr} = 0.04X_{Sgr} + 1.0$ kpc. The upper leading tidal tail has about 40% as many stars as the lower branch, but shows the same downward trend in star counts from $\Lambda_\odot = 300°$ to $\Lambda_\odot = 250°$. However, the upper-branch density falls precipitously by $\Lambda_\odot = 230°$. This is most apparent in the F-turnoff star counts. In the range $205° < \Lambda_\odot < 235°$ there are 12,653 F-turnoff stars in the lower branch, and none in the upper branch (after background subtraction).

These density distributions and ratios of relative numbers of K/M giant:BHB:F-turnoff stars will be of considerable use in modeling the Sgr stream, since the prediction of stellar number density can be used as a constraint, in addition to the position and velocity data that has so far been used.

12. The H-R diagram of the Sgr Stream

The SDSS/SEGUE spectroscopy give us the opportunity to look at the H-R Diagram of the Sgr tidal stream with much less contamination from main- sequence stars than the photometric H-R diagram in Figure 3; the drawback is that the spectra are not a complete sample and there are significant selection effects as a function of color.

We selected from the SDSS DR7 SppParams database table all of the objects with spectra, within the angular limits of the Sgr leading tidal tail in Figure 7, 9, and 11 (those figures use limits in Z_{Sgr}, but since we do not know the distance to each spectroscopic target we selected a similar area of the sky in $\Lambda_\odot, B_\odot$). We then selected all of the stars with low surface gravity, $1.0 < \log g < 3.75$, and within the velocity range of the leading tidal tail as a function of $\Lambda_\odot$. This resulted in a sample of 1,887 objects that are candidate Sgr stream stars at a variety of distances from the Sun.

Since the Sgr stream is at different distances at different places in the sky, we calculated a "corrected" apparent magnitude by adding the quantity $-5.0 * \log(d_{Sgr}(\Lambda_\odot)/30\text{kpc})$ to each g_0 apparent magnitude. This adjusts the apparent magnitude of each star in the Sgr stream to the apparent magnitude it would have if it were at 30 kpc.

The upper panel of Figure 19 shows the adjusted apparent g_0 magnitude as a function of $(g-r)_0$ The imprint of the SDSS/SEGUE selection function is discernable here (for example, SEGUE took spectra of a large number of G dwarfs near $(g-r)_0 = 0.5$). We can also clearly see the Sgr stream candidate HB stars at a corrected g_0 of 18, and the very red M-giant stream candidate stars at a corrected g_0 of about 16.5.

The lower panel of Figure 19 shows a color magnitude diagram for stars from Figure 12 that have velocities consistent with membership in the Sgr tidal stream. The BHB stars are similar, since they were spectroscopically selected. Our K/M-giant sample extends redder than the spectroscopically selected M giants. The SSPP does not prvide reliable surface gravities for stars redder than $(g - r)_0 = 1.3$, so they are not present in the upper panel's selected sample.

13. Discussion and Conclusions

From analysis of optical imaging and spectroscopy of stars in the complex Sagittarius tidal stream, we present new results on the stellar populations, velocities, metallicity distributions, and spatial and density distributions of the tidal debris stream. This information, combined with other Sgr stream data in the literature, can be used to constrain models for the stream orbit and thereby contribute to our knowledge of the shape of the Milky Way's dark-matter halo gravitational potential. Kinematic information is crucial to separating leading-tail candidates from trailing-tail candidates. Metallicity and stellar population information is important for distinguishing or identifying separate stellar populations, which may have be stripped at different times.

We conclude that:

(1) We can photometrically select the reddest K/M-giant stars in the Sgr dwarf tidal stream with SDSS ugr filters for objects down to about $g \sim 18.5$, corresponding to d= 80 kpc from the Sun. The tip of the M-giant branch in the Sgr dwarf tidal stream has an absolute magnitude of $M_{g_0} = -1.0$. The giant branch in the Sgr dwarf leading tidal tail is consistent with those of globular clusters with [Fe/H] of -1 ± 0.5. The 33 identified Sgr K/M giant stars have metallicities of -0.8 ± 0.2, as measured by the SDSS DR7 SEGUE Stellar Parameters Pipeline, but an independent determination of these giant star metallicities should be made.

(2) Following the technique of Majewski et al. (2003), we can trace the Sgr dwarf tidal stream over the entire SDSS+SEGUE imaging footprint. The positions of the K/M giants are consistent with the measured positions of Sgr BHB stars from Newberg et al. (2007).

(3) The line-of-sight velocities of BHB and K/M giant stars that are spatially coincident with the Sgr leading and trailing tidal tails are the same as those measured by Law, Johnston, & Majewski (2005). This indicates that the velocities are not seriously contaminated with other debris in the Virgo region, as (incorrectly) conjectured by Newberg et al. (2007).

(4) We measure the density of K/M-giant stars, HB stars, and F-turnoff stars as a function of angle along the Sagittarius dwarf tidal stream. Within our errors, the ratio of star counts in each of these star types is the same in both branches of the leading tidal tail and in the trailing tidal tail. The stellar density in the Sgr leading tidal tail decreases from the apogalactic turning point at $\Lambda_\odot \sim 300°$ going toward the Galactic anticenter, falling more sharply for the lower surface brightness, higher Galactic latitude branch. These density profiles can be used to aid in modeling of the tidal disruptions.

(5) The lower surface brightness tidal debris stream 'branch' that is parallel to the main leading tidal tail has velocities, metallicities, and relative densities of K/M-giant, BHB, and F-turnoff stars that are similar to the main Sgr leading tidal tail. Models that explain the upper branch as debris that has orbited the Galaxy at least one more time than the lower branch (leading tidal tail), or at least one less time (trailing tidal tail), must also explain the similarity in populations between these two debris streams. Alternatively, we suggest the two branches might be from debris that was stripped from the Sgr dwarf galaxy at similar times.

(6) A previously unknown, low-metallicity tidal debris stream that is spatially coincident with the Sgr South dwarf trailing tidal stream, but which exhibits a distinct metallicity and velocity profile, is identified and will be the subject of a future paper.

REFERENCES

Abazajian K., et al. 2009, ApJS, 182, 543.

Abazajian et al. 2003, AJ, 126,2081

Allende Prieto, C. et al. 2008 AJ, 136, 2070.

Allgood, B., Flores, R., Primack, J. Kravtsov, A. Wechsler, R., Faltenbacher, A. & Bullock, J. 2006 MNRAS 367, 1781.

An, D., Johnson, J. et al. 2008 ApJS, 179, 326.

Bell, E. F. et al. 2008, ApJ, 680, 295.

Bellazzini, M., Newberg, H. J., Correnti, M., Ferraro, F. R., & Monaco, L. 2006, å, 457, L21

Belokurov, V., Evans, N. W., Irwin, M. J., Hewett, P. C., & Wilkinson, M. I. 2006, ApJ, 637, L29

Belokurov, V. et al. 2006a, ApJ 642, L137.

Belokurov, V. et al. 2006b, ApJ 647, L111.

Belokurov, V. et al. 2007a, ApJ 658,337

Belokurov, V., et al. 2007, ApJ, 657, L89

Chou, M.-Y. et al. 2007, ApJ, 670, 346

Clem, J. L., Vanden Berg, D. A., Stetson, P. B. 2008 AJ 135, 682

Dehnen, W. & Binney, J. J. 1998, MNRAS, 298, 387

Duffau, S., Zinn, R., Vivas, A. K., Carraro, G., Mendez, R. A., Winnick, R., & Gallart, C. 2006, ApJ, 636, L97

Fellhauer, M., et al. 2006, ApJ, 651, 167

Fukugita, M., Ichikawa,T., Gunn, J. E., Doi, M., Shimasaku, K., Schneider, D. P. 1996, AJ, 111, 1758

Grillmair, C. J. 2008, arXiv:0811.3965

Grillmair, C. J. 2006a, ApJ, 645, L37

Grillmair, C. J. 2006b, ApJ, 651, L29

Grillmair, C. J., & Dionatos, O. 2006, ApJ, 643, L17

Grillmair, C. J., & Johnson, R. 2006, ApJ, 639, L17

Gunn, J. E. et al. 1998, AJ, 116, 3040

Gunn, J. E. et al. 2006, AJ, 131, 2332

Harrigan, M. J., Newberg H. J., Yanny, B., Beers, T.C., Lee, Y.S., & Re Fiorentin, P., in preparation

Helmi, A. et al. 2005, ApJ, 586, 195

Helmi, A. 2004, ApJ, 610, L97

Hogg, D. W., Finkbeiner, D. P., Schlegel, D. J., & Gunn, J. E. 2001, AJ, 122, 2129

Ibata, R. A., Gilmore, G., and Irwin, M. J. 1994, Nature, 370, 194

Ibata, R., Lewis, G. F., Irwin, M., Totten, E., and Quinn, T. 2001, ApJ, 551, 294

Ibata, R. A., Irwin, M. J., Lewis, G. F., Ferguson, A. M. N., & Tanvir, N 2003, MNRAS 340, L21

Ivezić, Z., et al. 2000, AJ, 120, 963

Ivezić, Z., et al. 2004, Astronomische Nachrichten, 325, 583

Johnston, K. V., Law, D. R., & Majewski, S. R. 2005, ApJ, 619, 800

Juric, M., et al. 2008, ApJ 673, 864.

Keller, S. C., Da Costa, G. S., & Prior, S. L. 2009 MNRAS, 394, 1045.

Layden, A. C., Hanson, R. B., Hawley, S. L., Klemola, A. R., & Hanley, C. J. 1996, AJ, 112, 2110

Law, D. R., Johnston, K. V. & Majewski, S. R. 2005, ApJ, 619, 807

Lee, Y. S. et al. 2008 AJ 136, 2022.

Lee, Y. S. et al. 2008 AJ 136, 2050.

Lenz, D. D., Newberg, H. J., Rosner, R., Richards, G. T., & Stoughton, C. 1998, ApJS, 119, 121

Majewski, S. R., Skrutskie, M. F., Weinberg, M. D., and Ostheimer, J. C. 2003, ApJ, 599, 1082

Martinez-Delgado, D., Penarrubia, J., Juric, M., Alfaro, E. J., Ivezic, Z. 2007, Ap. J. Suppl., 660, 1264

Martinez-Delgado, D., Gomez-Flechoso, M. A., Aparicio, A., Carrera, R. 2004, ApJ, 601,242

Moultaka, J., Ilovaisky, S. A., Prugniel, P., & Soubiran, C. 2004, PASP, 116, 693

Monaco, L., Bellazzini, M., Bonifacio, P., Buzzoni, A., Ferraro, F. R., Marconi, G., Sbordone, L., & Zaggia, S. 2006, A&A, 464, 201

Newberg, H.J., Yanny, B. & Willett, B.A. 2009, ApJ, submitted.

Newberg, H., Yanny, B., Cole, N., Beers, T. , Re Fiorentin, P., Schneider, D., and Wilhelm, R. 2007, ApJ, 668, 221.

Newberg, H., & Yanny, B. 2006, in JPC Conf. Ser.: Physics at the end of the Galactic Cosmic Ray Spectrum, ed. G. Thomson & P. Sokolsky, astro-ph/0507671

Newberg, H., & Yanny, B. 2005, in ASP Conf. Ser. 338: Astrometry in the Age of the Next Generation of Large Telescopes, ed. P. K. Seidelmann & A. K. B. Monet, 210, astro-ph/0502386

Newberg, H., Yanny, B., et al. 2003, ApJ, 596, L191

Newberg, H., Yanny, B., et al. 2002, ApJ, 569, 245

Odenkirchen, M. et al. 2006, AJ, 126, 2385

Parker, J. E., Humphreys, R. M., & Larsen, J. A. 2003, AJ, 126, 1346

Pier, J. R., Munn, J. A., Hindsley, R. B., Hennessy, G. S., Kent, S. M., Lupton, R. H., and Ivezić, Z. 2003, AJ, 125, 1559

Savage, C., Newberg, H. J., Freese, K., & Gondolo, P. 2006, Journal of Cosmology and Astroparticle Physics, 7, 3

Schlegel, D.J., Finkbeiner, D.P., & Davis, M. 1998, ApJ, 500, 525

Searle, L., & Zinn, R. 1978, ApJ, 225, 357

Skrutskie, M. F., et al. 2006, AJ, 131, 1163

Smith, J. A. et al. 2002, AJ, 123, 2121

Stoughton, C., et al. 2001, AJ, 123, 485

Tucker, D., et al. 2006, Astronomische Nachrichten, 325, 583

Vivas, A. K. et al. 2001, ApJ, 554, L33

Vivas, A. K., Zinn, R. & Gallart, C. 2005, AJ, 129, 189.

Wilhelm, R., Beers, T. C., & Gray, R. O. 1999, AJ, 117, 2308

Willett, B. A., Newberg, H. J., Zhang, H., Yanny, B., & Beers, T. C. 2009, arXiv:0901.4046

Xu, Y., Deng, L. C. & Hu, J. Y. 2006, MNRAS, 368, 1811

Xu, Y., Deng, L. C. & Hu, J. Y. 2007, MNRAS, 379, 1373.

Yanny, B., et al. 2009, AJ, 137, 4377.

Yanny, B., Newberg, H. J., et al. 2000, ApJ, 540, 825

Yanny, B., Newberg, H. J., et al. 2003, ApJ, 588, 841

York, D.G. et al. 2000, AJ, 120, 1579

Zinn, R., Vivas, A. K., Gallart, C. & Winnick, R. 2004, ASP Conf. Series, 327, 92
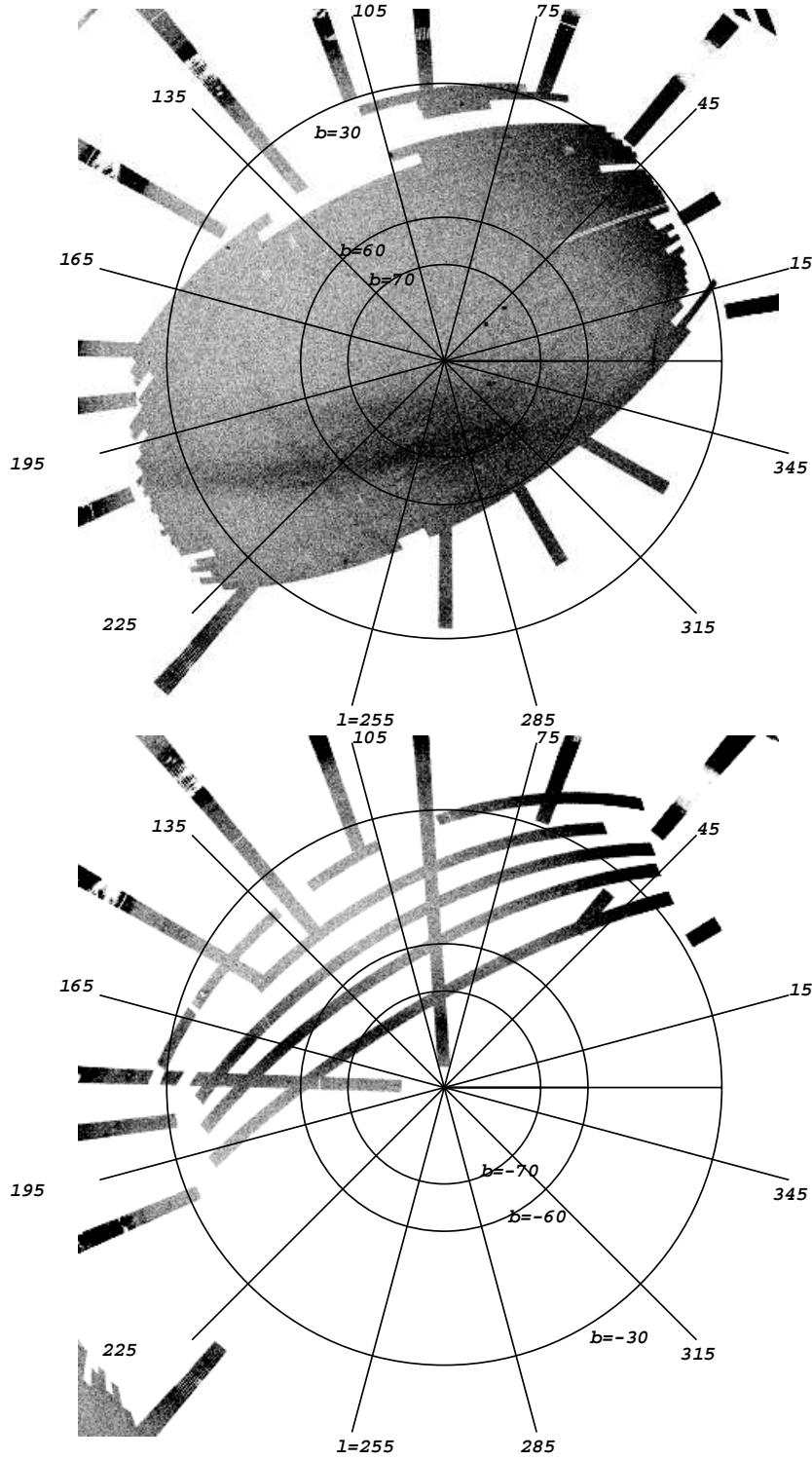
Fig. 1.— The upper panel shows the density of photometrically selected F-turnoff stars with $21 < g_0 < 22$ in the North Galactic Cap. In addition to the prominent Sagittarius stream, note the Orphan stream and Pal 5 are visible at $(l, b) = (195° : 255°, 50°)$ and $(l, b) = (1°, 45°)$, respectively. Note that the Sgr leading tidal tail, which dominates the star counts in this figure, appears to be bifurcated; the main leading tidal tail is at lower Galactic latitudes and there is a fainter, nearly parallel tidal tail at higher Galactic latitudes. The lower panel shows the density of photometrically selected F-turnoff stars in the South Galactic Cap. Note the strong Sagittarius trailing tail of F stars running from $(l, b) = (100°, -85°)$ to $(170°, -40°)$.
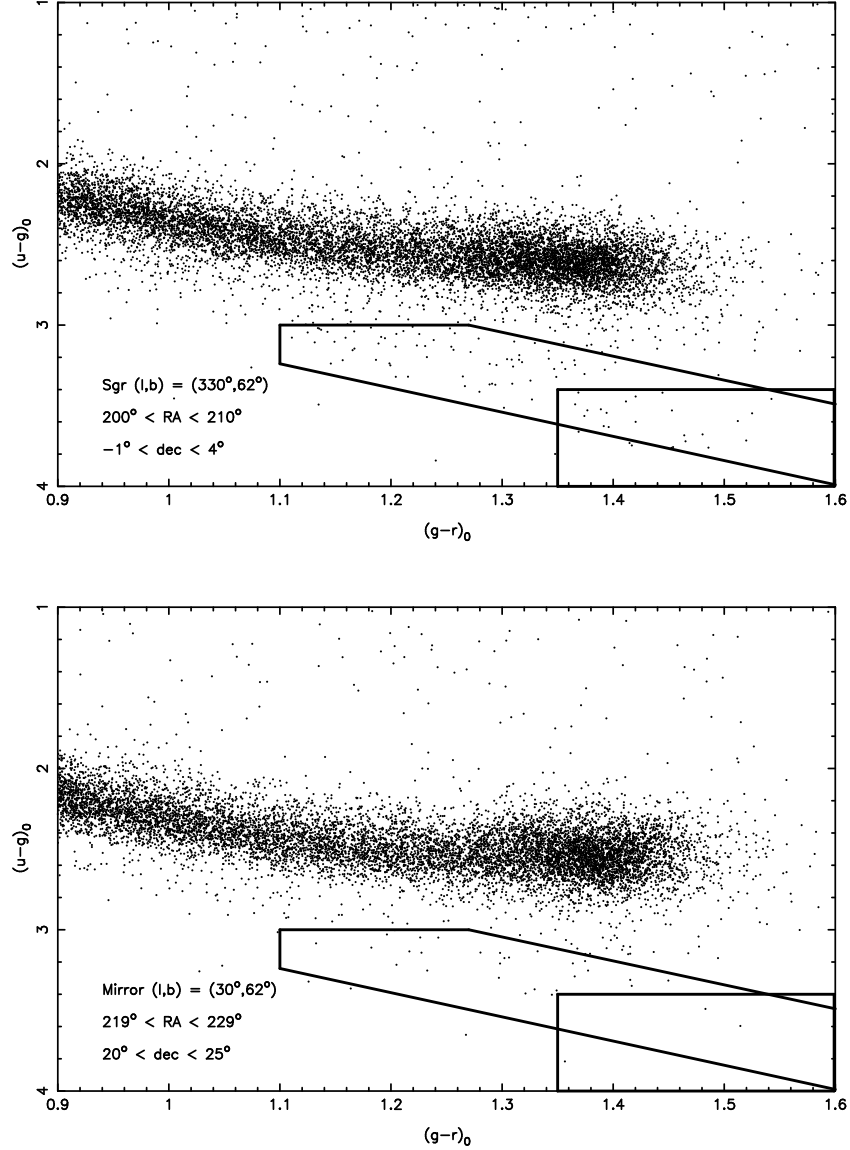
Fig. 2.— Selection of K/M giants using the fact that they have very red $(u - g)_0$ colors which extend redward of the $(u - g)_0$ M-dwarf stellar locus for $g - r$ redder than 1.1. Upper panel: $((g-r)_0, (u-g)_0)$ color-color diagram red stars in a 50 square degree box covering the Sagittarius North tidal stream leading tail. Note the excess of stars below the locus at red $(u - g)_0$: these are distant K/M giant candidates. The outlined selection boxes are described in the text. Lower panel: Same size selection box as above, but in a mirror image direction on the sky in Galactic l with respect to the Galactic center. There are significantly fewer K/M giant candidates, especially in the lower-right rectangular 'very red' selection box.
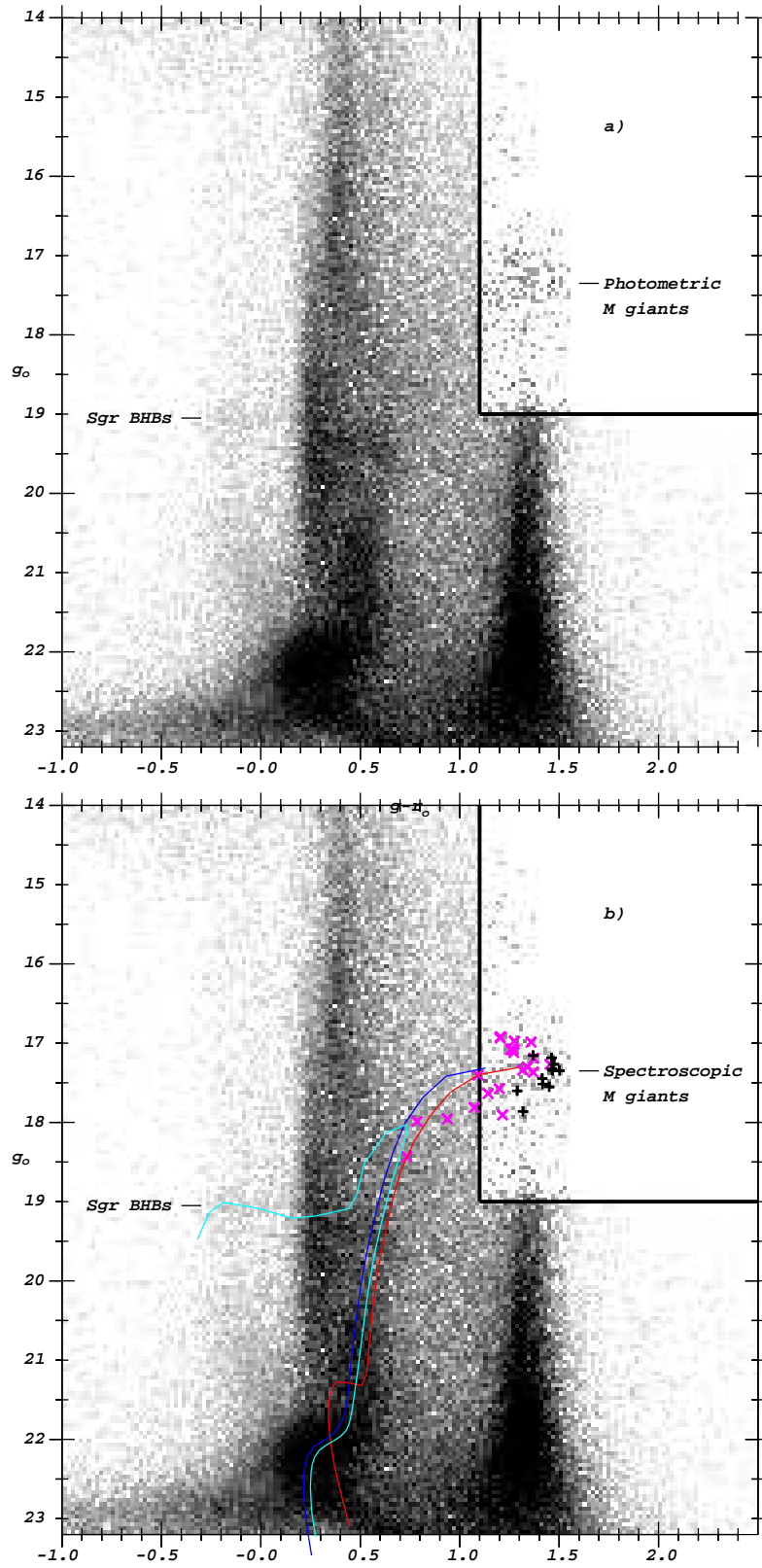
Fig. 3.— The upper panel, a), of this $(g - r)_{0}$, g_{0} color-magnitude Hess diagram is reproduced from Newberg et al. (2002), Figure 5, updated with DR7 data. It covers the area $(\alpha, \delta) = (200 : 225°, -4 : 1°)$. The inset in the upper right consists only of candidate K/M-giant stars which pass the strip cut color selection (larger diagonal box) of Figure 2. The relative number of stars in the inset is multiplied by a factor of 10 compared with the main panel to highlight the end of the giant branch. In the lower panel, b), fiducial sequences from clusters M 3 with [Fe/H] = −1.5, (cyan), including a BHB and M 92 with [Fe/H] = −2.1 (blue), are shifted in magnitude to match the turnoff of Sagittarius stream, and superimposed. M 71 with [Fe/H] = −0.8 (red) is shifted to match the giant branch. Spectroscopically confirmed giants are marked with a magenta x (bluer K giants, with no TiO bands observed) or with a black + (redder M giants, with strong TiO).
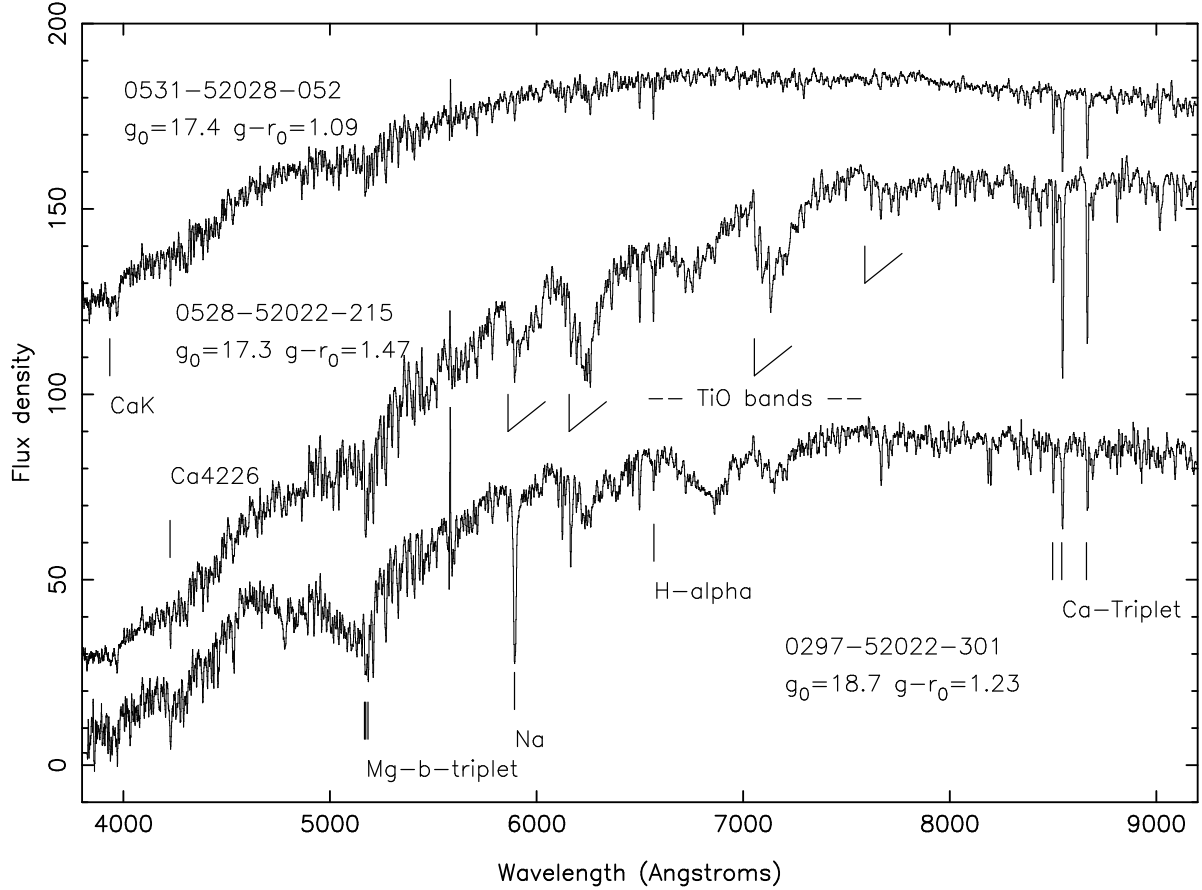
Fig. 4.— Sample K and M star spectra: Three SDSS red-star spectra from the direction of sky indicated in Figures 1 and 2. The upper spectrum (offset by 120 units) is a K giant with $(g - r)_0 = 1.09$; note the weak Mg triplet near 5200Å and the weak Ca 4226Å. The middle spectrum, (offset by 20 units) is a very red M giant with $(g - r)_0 = 1.47$; note the weak Mg triplet, weak Na 5896, yet strong TiO bands. The lower spectrum is an M dwarf, with strong Ca 4226, Mgb/H, and Na I features. The giants are ~ 44 kpc distant while the dwarf is at about $d = 1$ kpc.
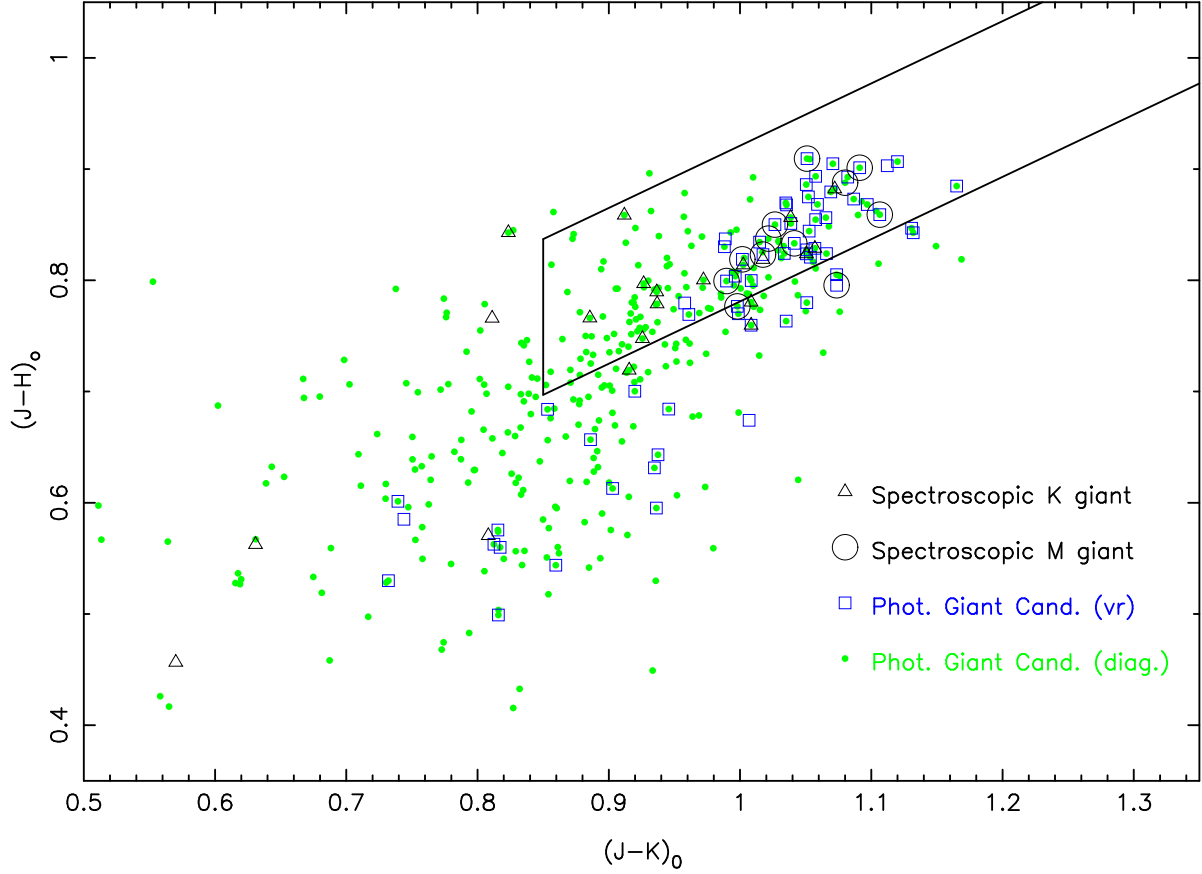
Fig. 5.— A 2MASS IR color-color diagram of Sgr tidal stream K- and M-giant candidates that were photometrically selected in SDSS ugr filters, as well as spectroscopically confirmed K and M giants. The parallelogram box is that of Majewski et al. (2003), who originally used 2MASS giants to trace the Sgr stream around the Milky Way. The large open black circles are SDSS spectroscopically confirmed M giants, the triangles are spectroscopically confirmed K giants (giants with no TiO bands), the filled (green) circles are Figure 2, upper plot, strip-cut photometric candidates, and the open (blue) squares are very red ugr candidates from the upper panel in Figure 2. Our selection has strong overlap with the M-giant selection of Majewski et al. (2003).
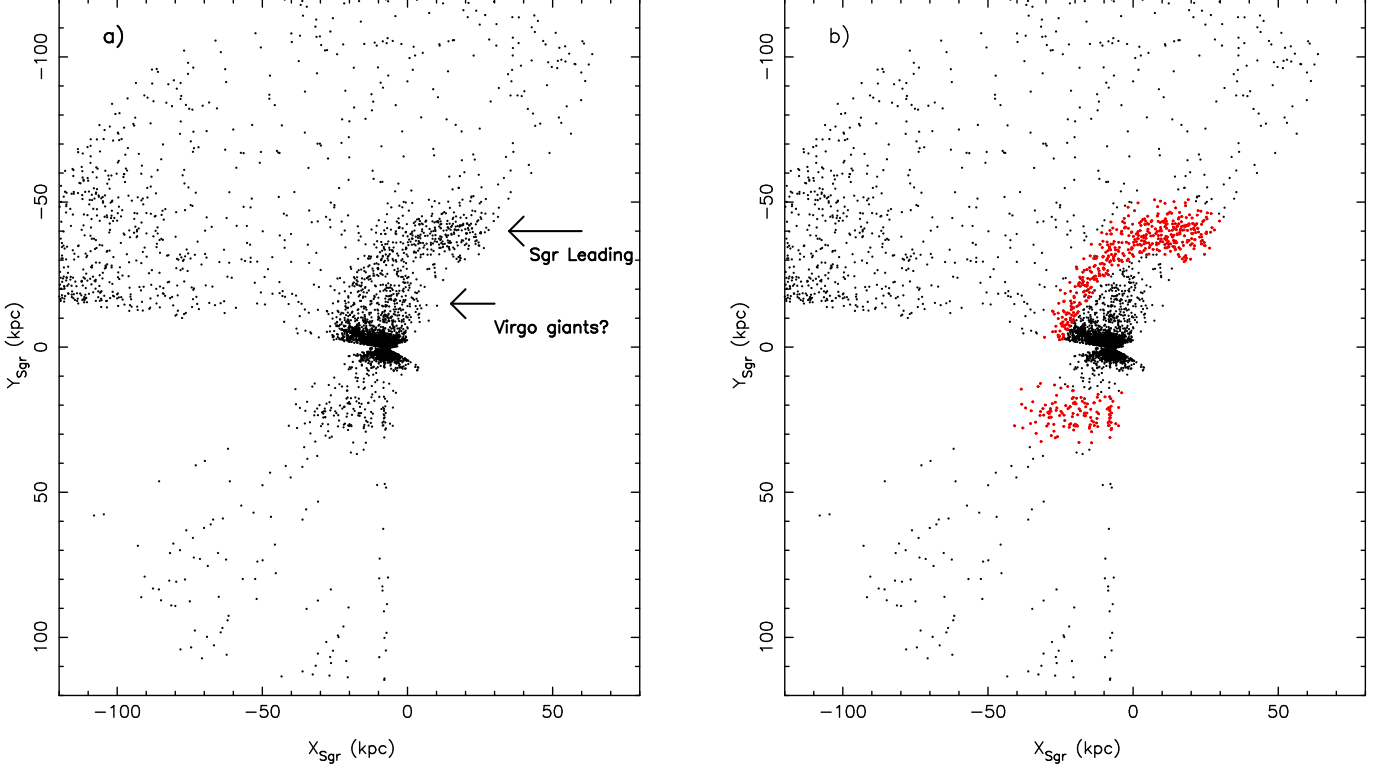
Fig. 6.— The left panel shows the color-selected K/M-giant candidates from all SDSS+SEGUE imaging data within 5 kpc of the Sgr dwarf orbital plane. The right panel shows the same stars, except the stars selected by position in the Sgr leading and trailing tidal streams are colored red. The coordinates are X_{Sgr}, Y_{Sgr}, and Z_{Sgr} as defined in Majewski et al. (2003). Y_{Sgr} is close to the $-Z$ axis in Galactic coordinates. The axis $+X_{Sgr}$ points approximately in the direction of the Galactic Center, as viewed from the Sun. The Galactic plane cuts through the figure at $Y_{Sgr} = 0$.
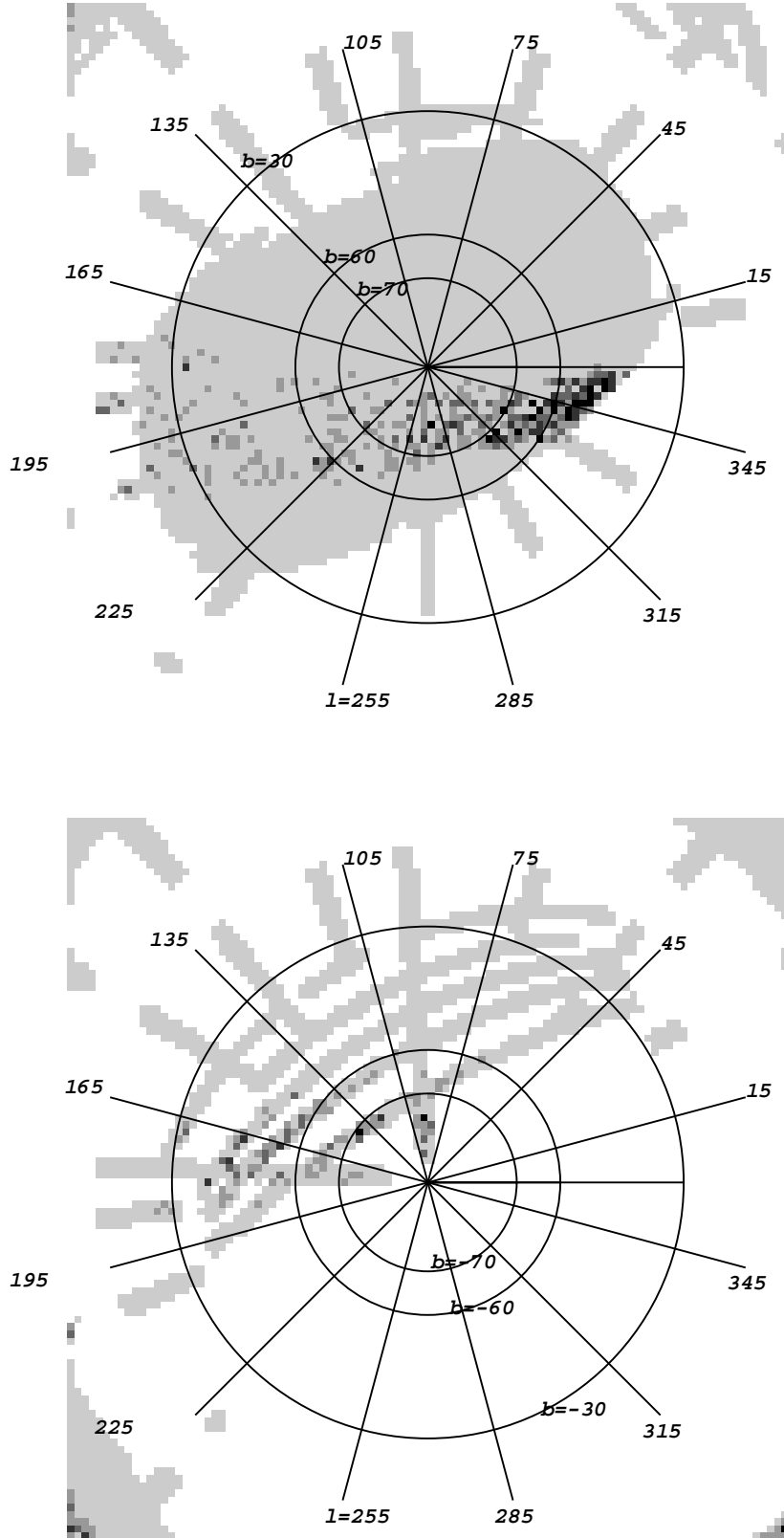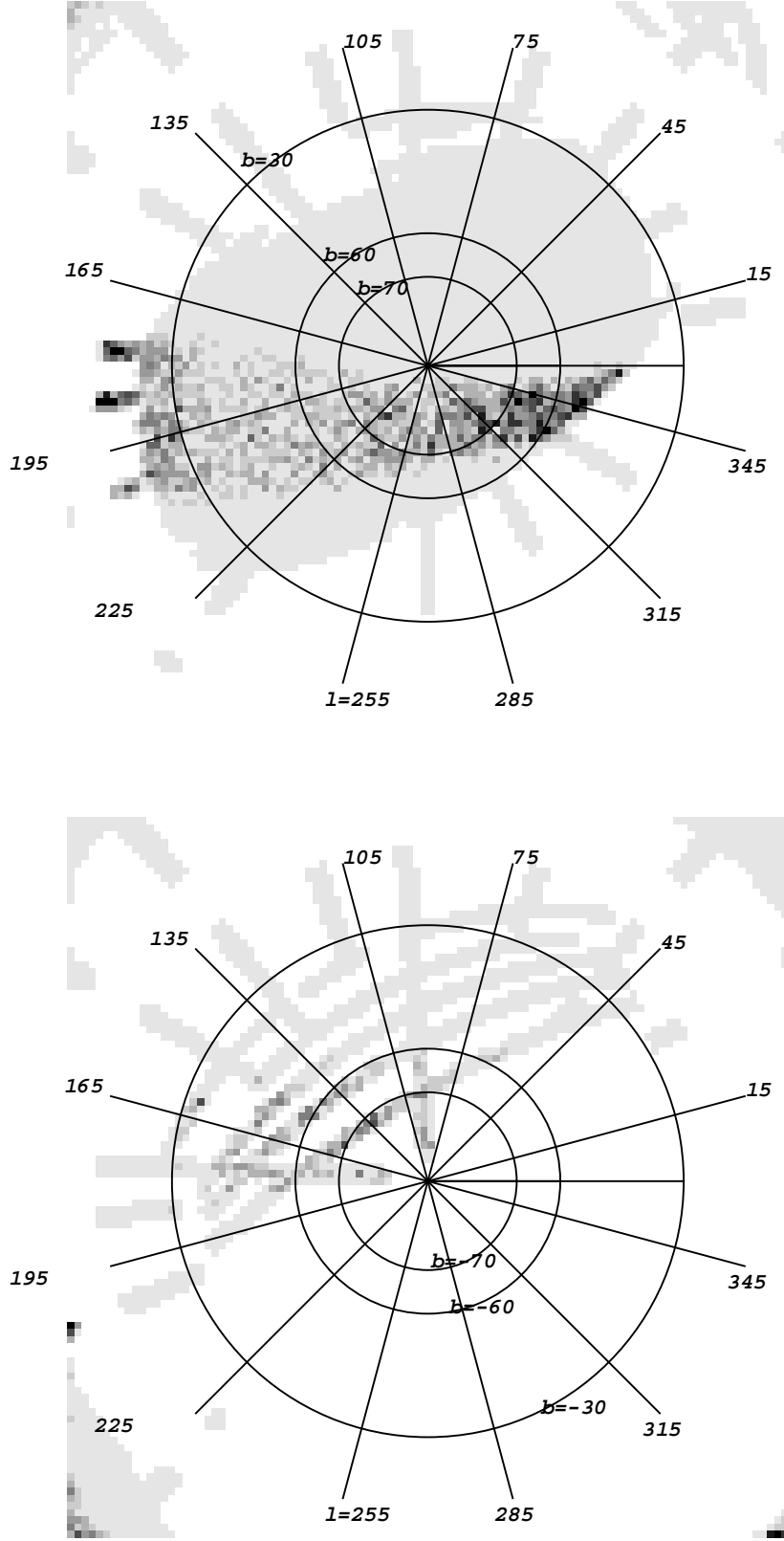
Fig. 7.— Galactic (l, b) polar plots showing the location of Sgr K/M giants colored red in Figure 6. The entire SDSS+SEGUE footprint is indicated in gray. The upper panel shows stars in the North Galactic Cap. Since the Sgr stream passes closer to the Sun on the left, the angular extent on the sky is wider there. The density of K/M-giant candidates is strongest at the right of the figure, near $\Lambda_\odot = 300°$, closest to the Sgr dwarf itself (not shown). The lower panel shows stars in the South Galactic Cap. Note the presence of K/M giants in the Southern Sgr trailing tidal stream near $l = 180°$.
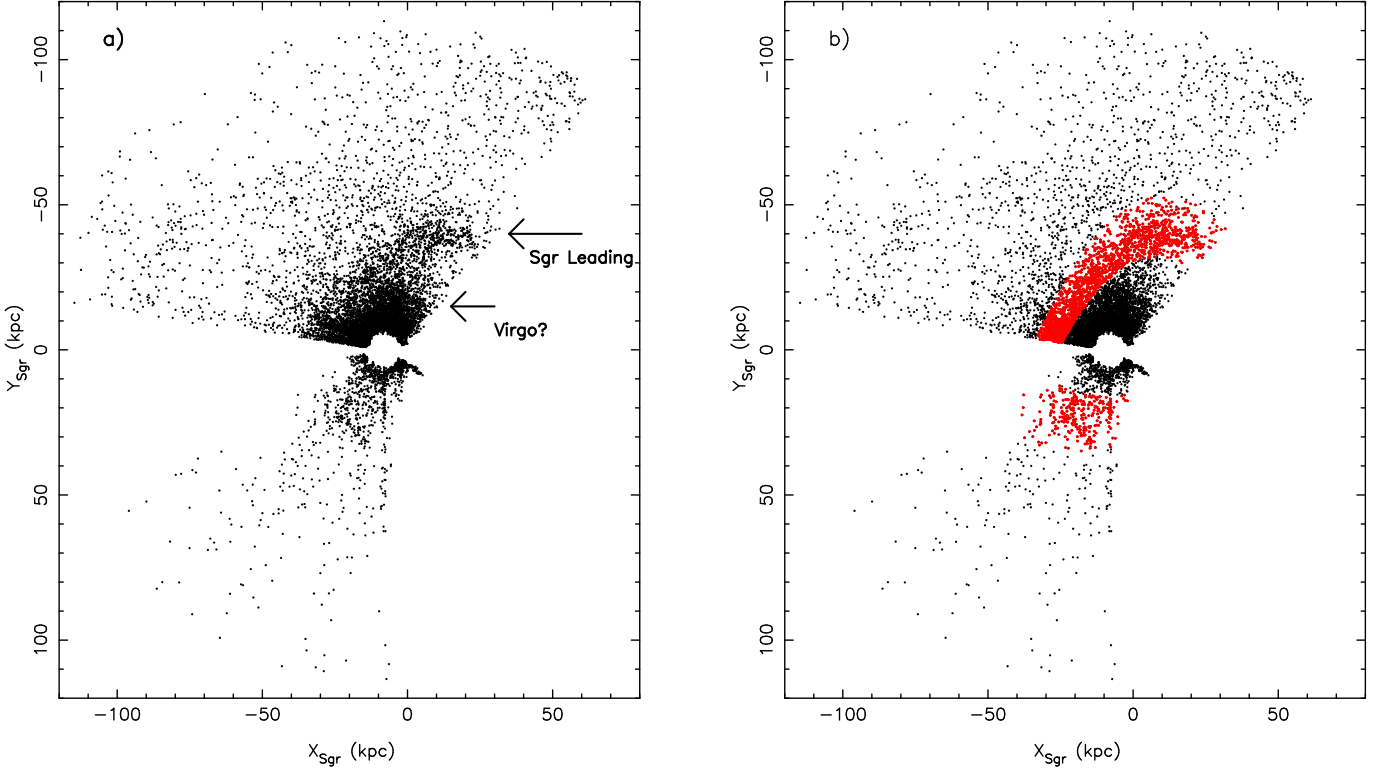
Fig. 8.— Sgr BHB star selection
Similar to Figure 6, except photometrically selected BHB stars are shown instead of K/M giants. The left panel shows the positions of BHB stars within 5 kpc of the Sgr stream orbital plane. The right panel shows the stars that are candidate Sgr stream stars. They were selected in exactly the same positions in the Galaxy as the K/M giants in Figure 6, assuming that BHB stars are intrinsically 1.7 magnitudes fainter in g than the K/M giants. Notice that the background contamination is higher for BHB stars, particularly close to the Sun.

Fig. 9.— Galactic (l, b) polar plots showing the location of Sgr BHBs colored red in Figure 8. The entire SDSS+SEGUE footprint is indicated in gray. The upper panel shows the North Galactic Cap and the lower panel shows the South Galactic pole. The features are very similar to the Figure 7 polar density plot of Sgr stream K/M giants, except that we see a strong excess of BHB stars near the anticenter in the upper panel. These stars are not associated with the Sgr dwarf tidal stream.
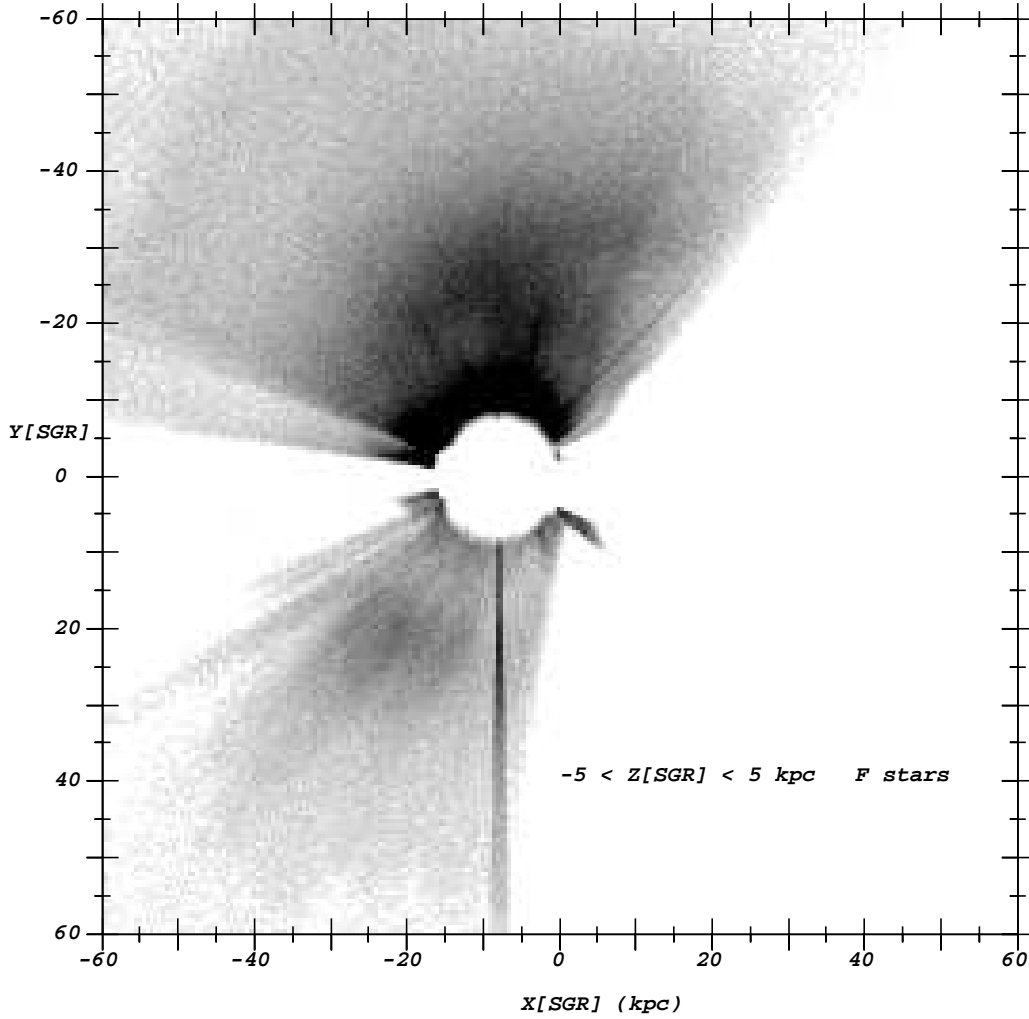
Fig. 10.— Sgr F-turnoff star selection.
Similar to Figures 6 and 8, but showing the density of photometrically selected F-turnoff stars within 5 kpc of the Sgr dwarf orbital plane. Since the density of F stars is some 60 times that of BHBs, we use a gray scale density (Hess) diagram rather than plotting individual stars. Radial features in this diagram are due to incompleteness, star clusters, or calibration errors (often due to reddening correction). The dark radial stripe in the south is due to higher completeness in the region of a SEGUE imaging stripe at constant Galactic longitude. We lose completeness of F-turnoff stars at about 40 kpc from the Sun. in the north, we see the Sgr dwarf leading tidal tail arcing over the Virgo Overdensity. We can also see the Sgr trailing tidal tail in the south.
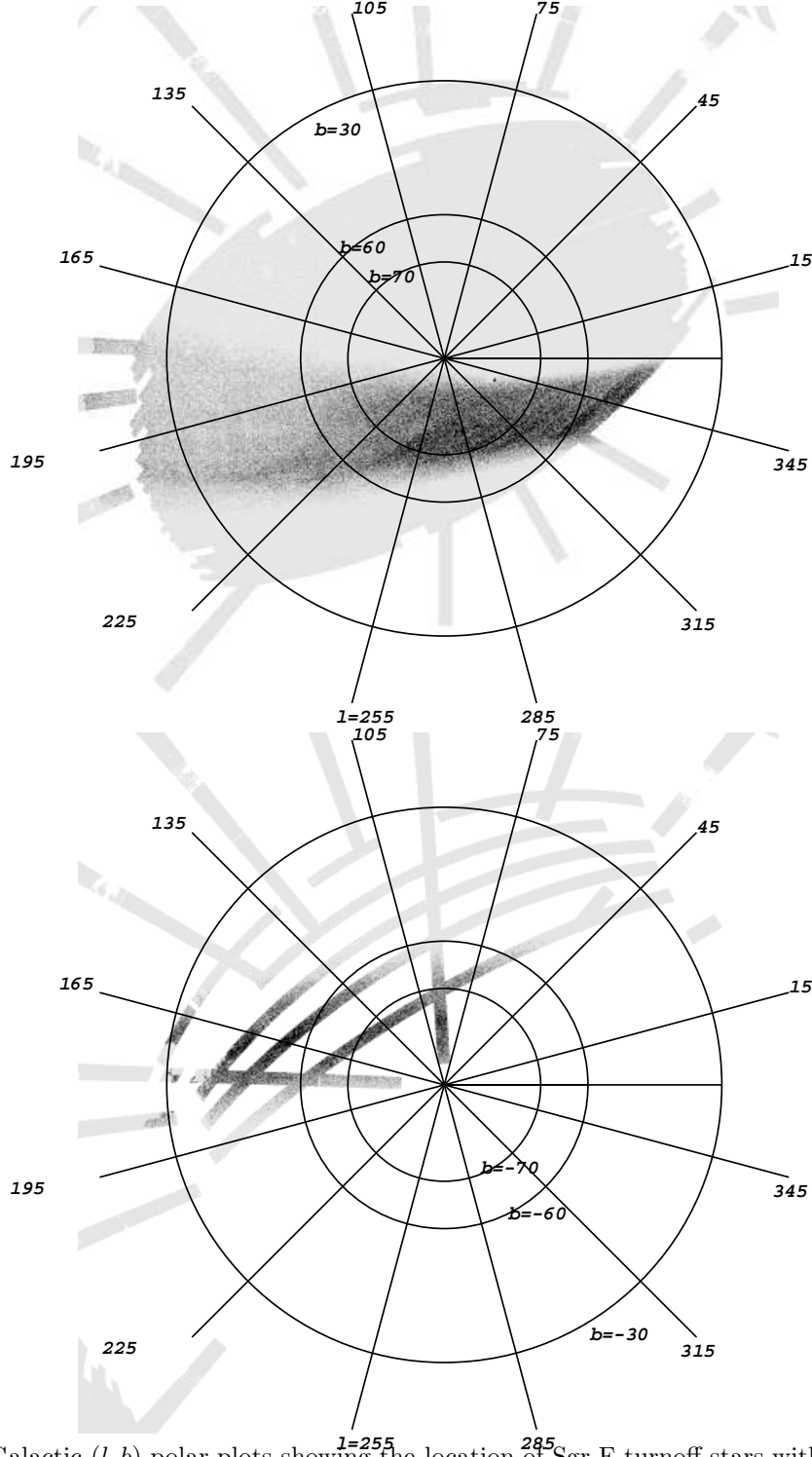
Fig. 11.— Galactic (l, b) polar plots showing the location of Sgr F-turnoff stars with $19 < g_0 < 23.5$ and $|Z_{Sgr}| < 5$ kpc, similar to that for K/M giants and BHBs in in Figures 6 and 8, assuming all of the F-turnoff stars are 5.2 magnitudes fainter than the K/M-giant stars. Since there is actually a very broad range of F-turnoff star absolute magnitudes, some stars may be missed in this selection. The entire SDSS+SEGUE footprint is indicated in gray. The upper panel shows stars in the North Galactic Cap, and the lower panel shows stars in the South Galactic Cap.
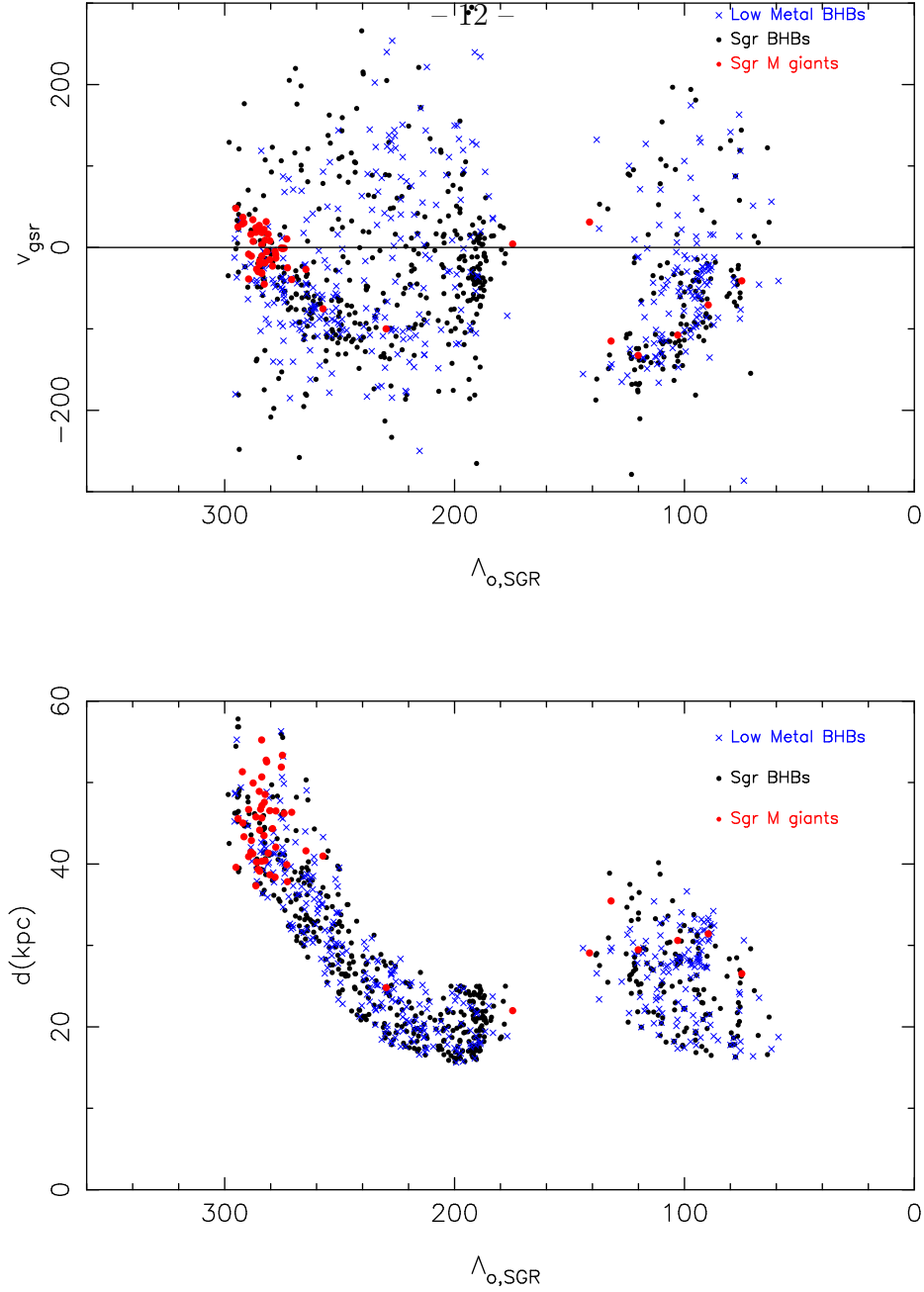
Fig. 12.— The top panel shows line-of-sight, Galactic standard of rest velocities, v_{gsr}, for all HB stars with SDSS/SEGUE spectra (selected as stars with $-0.3 < (g-r)_0 < 0.35$ and $1 < \log g < 3.75$) that are within 5 kpc of the Sgr dwarf orbital plane, and spatially coincident with the Sgr stream. We also show those photometrically selected K/M giant stars for which with SDSS+SEGUE spectra were taken (not many, and over a small area of sky). This plot mirrors that of Figure 12 in Law, Johnston, & Majewski (2005). The angle $\Lambda_{\odot,SGR}$ increases along the Sgr tidal stream, as defined in Majewski et al. (2003). The HB stars are divided into low metallicity ([Fe/H]$_{WBG}$ < -1.9, indicated with blue crosses), and high metallicity ([Fe/H]$_{WBG}$ > -1.9, filled black dots), samples. We find K/M giants (red dots) and both low- and high-metallicity BHB stars in the Sgr dwarf tidal stream. BHBs in the Virgo overdensity are apparent at $\Lambda_\odot = 230°$, $v_{gsr} = 130$ km s^{-1}. A new stellar stream is apparent in low-metallicity BHB stars near $\Lambda_\odot = 100°$, $v_{gsr} = -50$ km s^{-1}. The lower plot shows the estimated distances for each of the stars in the upper plot as a function of $\Lambda_\odot$. The newly identified low-metallicity stream has a very narrow distance distribution that rises toward the right in the lower panel.
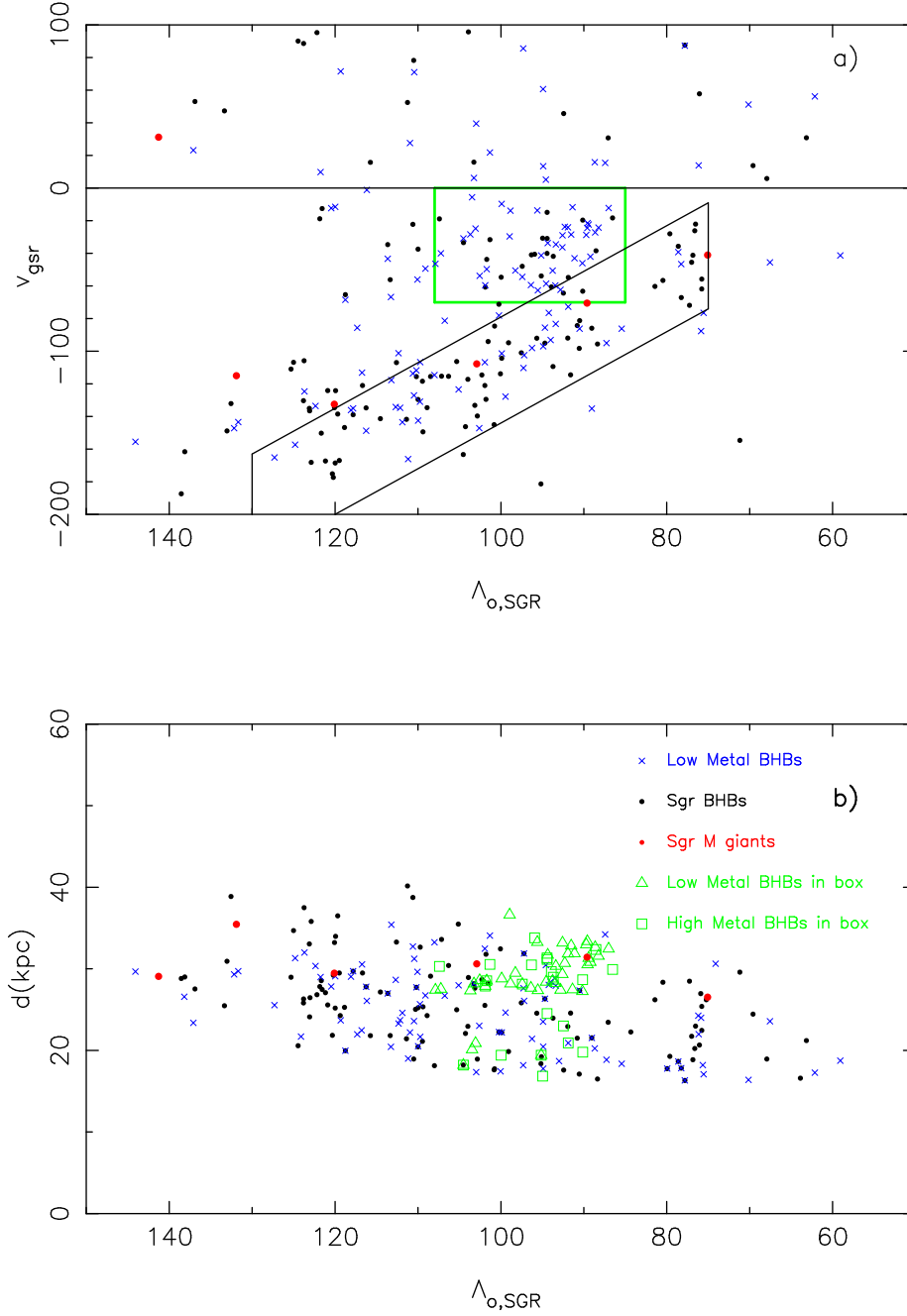
Fig. 13.— Same as Figure 12, except focusing on the South where a possible new stream is visible, distinct from the Sgr trailing tidal tail. The rectangular box in the upper panel, a), outlines the area of sky where the new stream is prominent in low-metallicity BHB stars. The diagonal box shows where the Sgr south trailing tidal tail is most prominent, containing stars of mixed metallicity. Note the ratio of low- to high-metallicity BHB stars is very different between the two outlined regions. In the lower panel, b), distances to all BHB stars from the rectangular box in the upper panel are plotted in green triangles (low metallicity) and squares (high metallicity). Note that these BHBs have a different distance distribution with $\Lambda_\odot$ than the Sgr tidal tail stars.
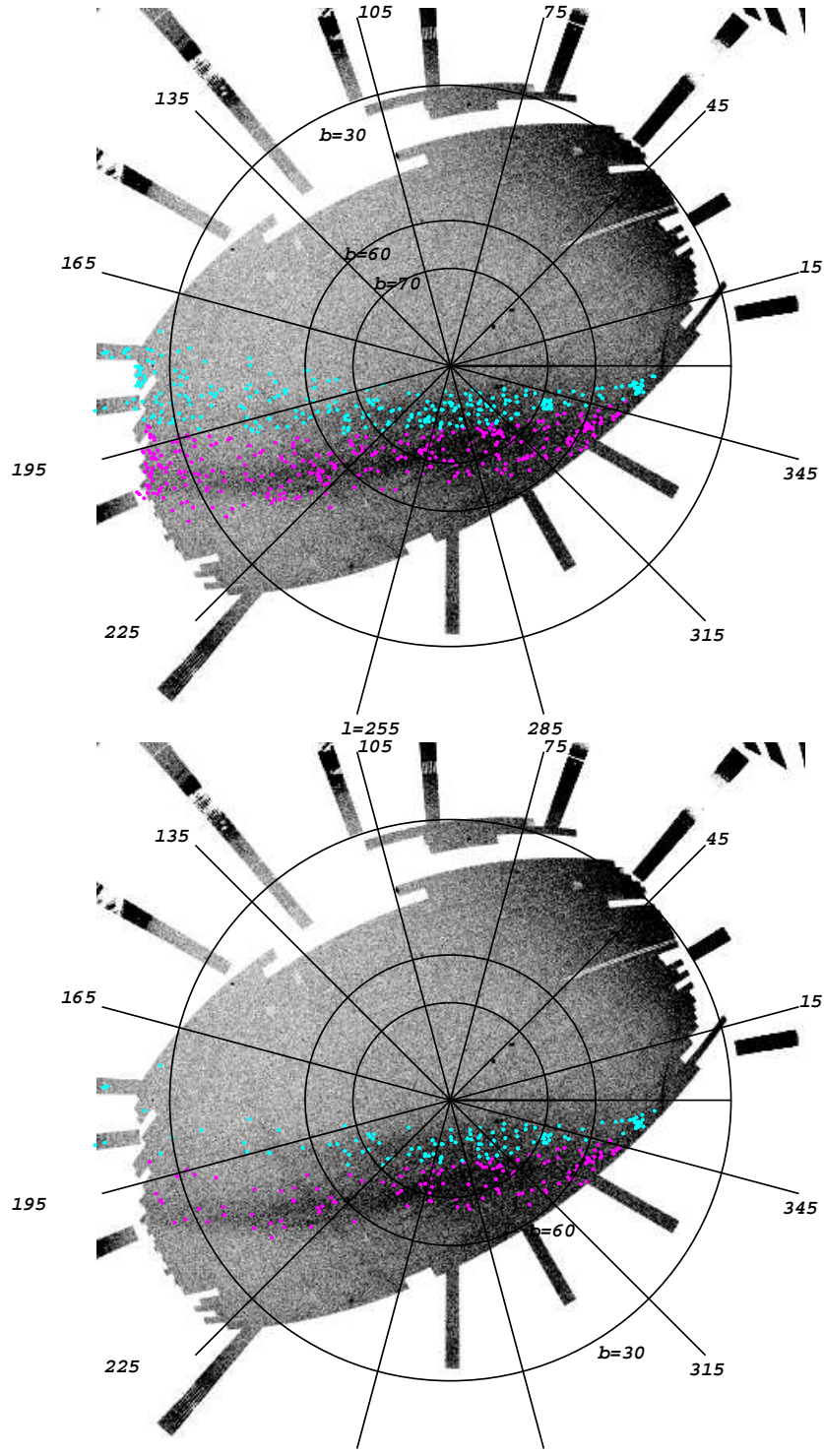
Fig. 14.— The upper panel shows the available HB spectra that are spatially coincident with the Sgr leading tidal tail; spectra that are candidates for the upper branch are shown in cyan and candidates for the lower branch are shown in magenta. The lower panel shows the subset of the HB spectra that have the correct velocities to be Sgr dwarf tidal debris. The sparse sampling of the lower, main leading tidal tail is a selection effect. The (l, b) locations of the spectra with the correct velocities for Sgr stream stars (shown in the lower panel) suggest that the two stream branches grow further apart (in angle) as they approach the Galactic anticenter.
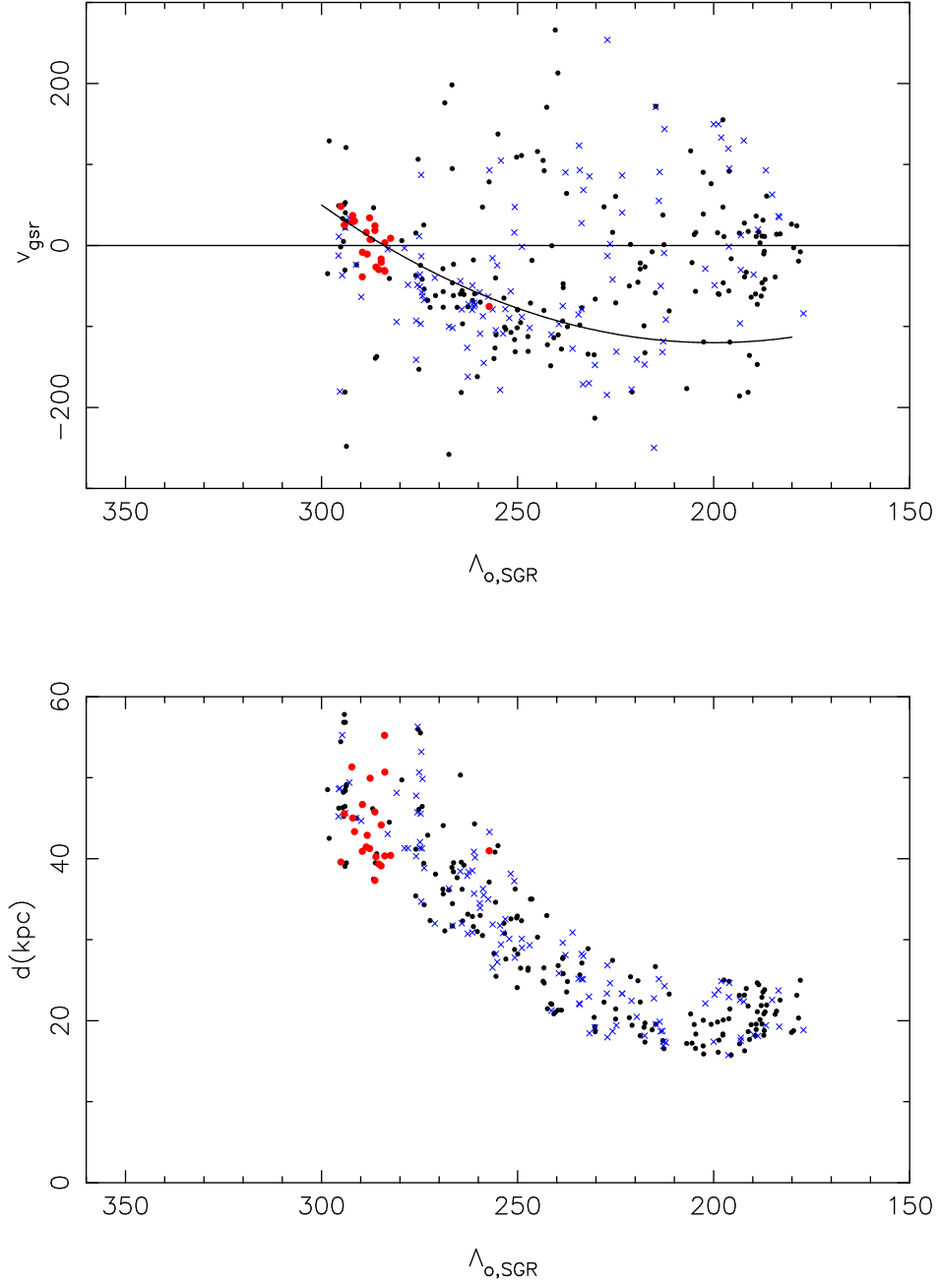
Fig. 15.— Velocities of Sgr leading tidal tail, upper branch.
Subsets of stars in Figure 12 that are in the upper branch of the Sgr leading tidal tail, with $Z_{Sgr} > 0.04X_{Sgr} + 1.0$, are shown. Two lines that approximately trace the velocities of the Sgr dwarf tidal debris are shown for reference.
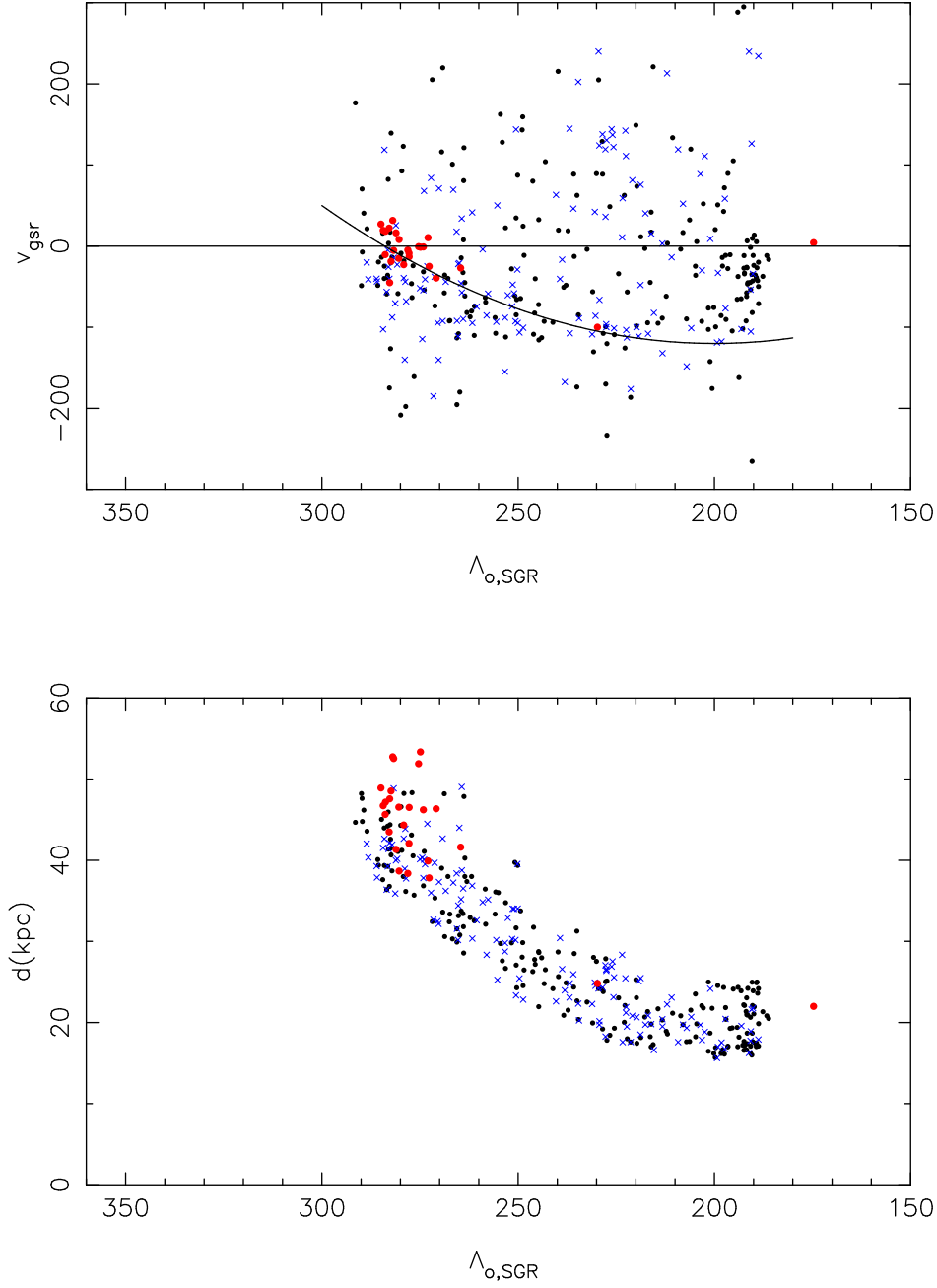
Fig. 16.— Velocities of Sgr leading tidal tail, lower branch.
Subsets of stars in Figure 12 that are in the lower, main branch of the Sgr leading tidal tail, with $Z_{Sgr} < 0.04X_{Sgr} + 1.0$, are shown. Two lines that approximately trace the velocities of the Sgr dwarf tidal debris are shown for reference. Note that the velocity distribution appears to be identical to the velocity distribution for the upper branch (Figure 15). The K/M giants at slightly different $\Lambda_\odot$ due to a selection effect (we have K/M-giant spectra over a very small area of the sky).
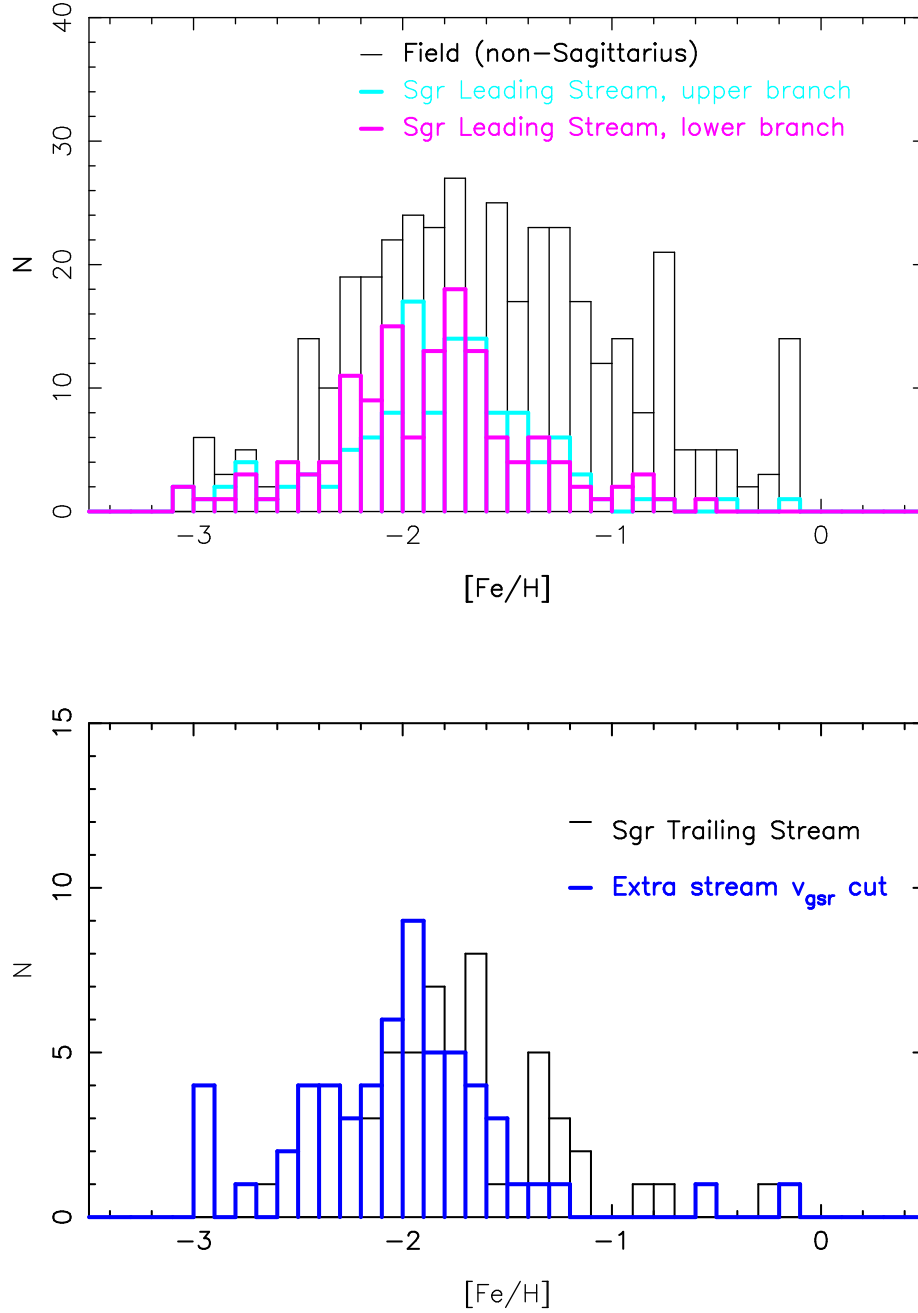
Fig. 17.— The upper panel shows the metallicity distribution of spectroscopically selected stars in the Sgr leading tidal tail upper branch (cyan) and lower branch (magenta). In black we show the distribution of metallicities for all spectroscopically selected HB stars that are spatially coincident with the Sgr stream, but do not have the correct velocities to be Sgr tidal debris. There is no significant distinction between the upper and lower branch metallicity distributions. The lower panel shows the metallicity distribution of the HB stars in the trailing tidal tail (black) along with the metallicity distribution of the HB stars in the newly discovered tidal stream (selected with $-71 < v_{\mathrm{gsr}} < 0$ km s^{-1} and $85° < \Lambda_\odot < 130°$). The metallicities in the new stream are lower than the average Sgr HB star. The spikes for HB metallicities at [Fe/H] $= -3.0$ are spurious.
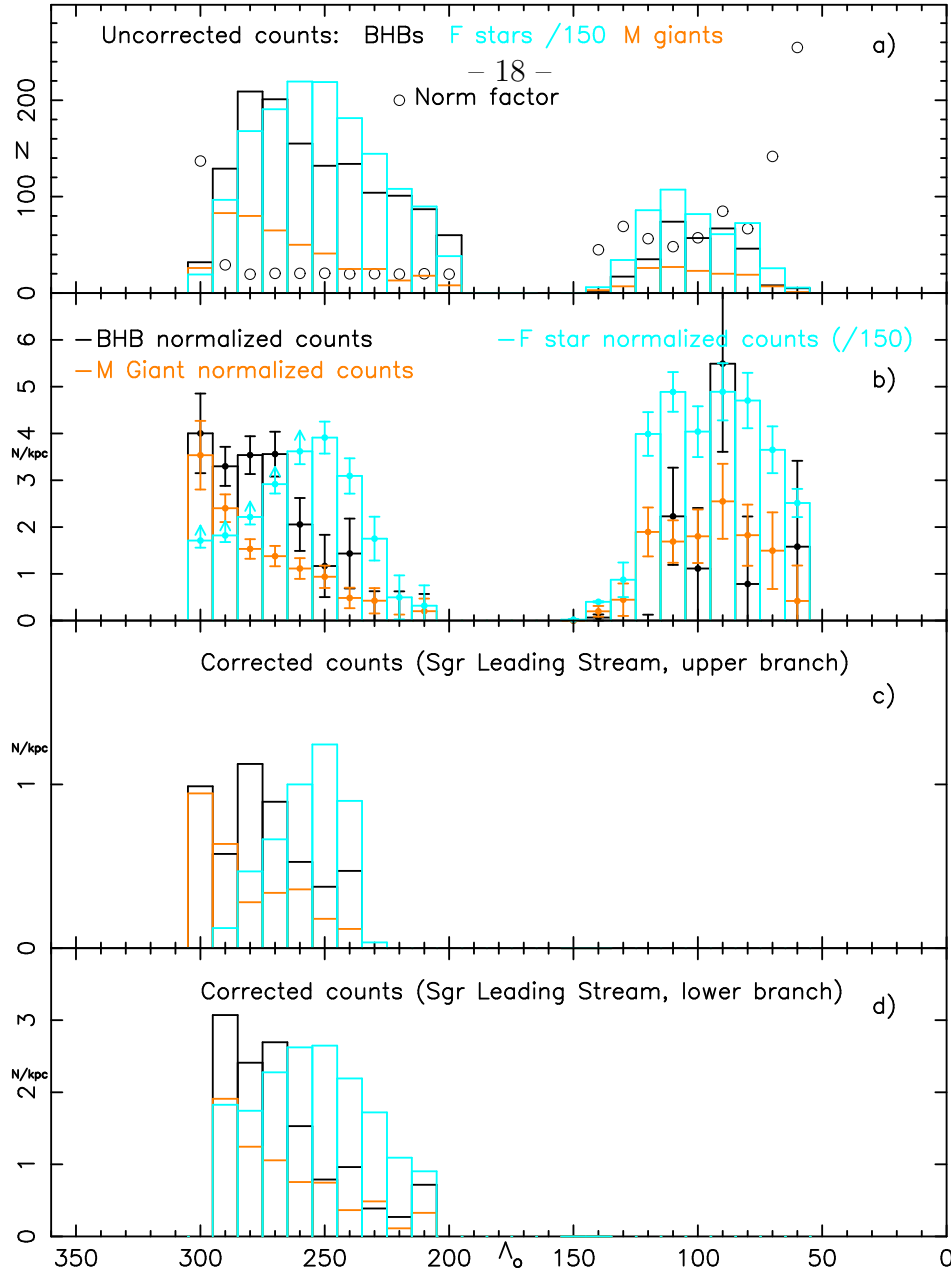
Fig. 18.— The top panel, a), shows the raw number counts of stars in each photometrically selected category, in ten degree angular bins along the Sgr dwarf tidal stream in $\Lambda_\odot$ (F-star counts are divided by 150 in all panels). The black open circles indicate the normalization factor (multiplied by 20 so that it is visible on the plot) that the bin will be multiplied by to account for the incompleteness of the data in that bin. The second panel, b), shows the star counts after they have been multiplied by the normalization factor, background subtracted, and divided by the distance to the Sgr tidal stream at that angular position in the sky. Note that since the F-turnoff stars in the Sgr stream are too faint to be observed in SDSS data in the first five bins, we have only lower limits for the F-turnoff star number counts on the left side of the plot. Notice that the ratio of K/M-giant stars to HB stars to F-turnoff stars is constant within the errors of the plot. The density of the leading tidal tail decreases from the left side of the plot toward decreasing $\Lambda_\odot$. The density along the observed portion of the Sgr trailing tidal tail is roughly constant. The lower two panels show the data in the leading tidal tail, split by upper, c), and lower, d), branches. The normalization for each bin was recalculated, and the subtracted background was scaled by the fraction of the stream width that is in each branch in each bin. There is no apparent difference in the ratio of K/M giants to BHB stars to F-turnoff stars. The upper leading tidal tail has less than half the density, and appears to end abruptly at $\Lambda_\odot \sim 235°$, however we note that bins where the background subtraction results in negative stream counts have been supressed.
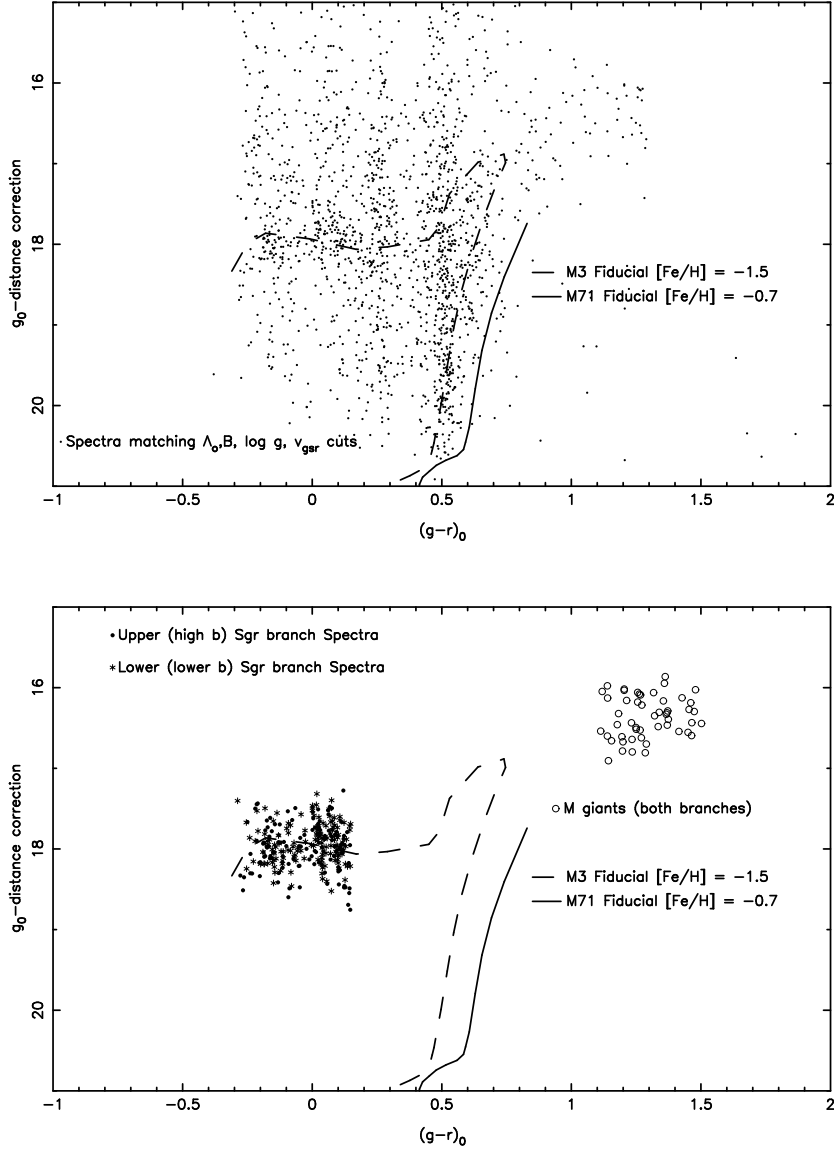
Fig. 19.— We selected all stellar spectra in SDSS DR7 within the angular limits of the Sgr leading tidal tail that have low surface gravity and velocities consistent with Sgr tidal debris. We adjusted the apparent magnitude of each star, based on its $\Lambda_\odot$ coordinate, so that if it is at the distance of the Sgr stream in that direction it would be shifted to 30 kpc. This should give us a Sgr blue horizontal branch at an adjusted g_0 of 18.1 and an K/M-giant branch at an adjusted g_0 of 16.4. In the top panel, we show the adjusted color-magnitude diagram for these stars, which does show the horizontal branch and K/M-giant branch of Sgr. The large number of counts at $(g-r)_0 = 0.5$ is due to the color selection for SEGUE spectra that favors this color range. The fiducial sequences for M 3 and M 71 (An et al. 2008), shifted to 30 kpc, are shown for reference. The lower panel shows the Sgr HB and K/M giant stars from Figure 12 that are at the correct velocities for Sgr tidal debris. The BHB selection is very good. Since log g is not measured reliably for M giants with $(g-r)_0 > 1.3$ in SDSS, they cannot be spectroscopically selected and are therefore absent in the top panel. Our lower panel K/M giant candidates are spectra that were selected by their photometric indices.